UWB OFDM SYNTHETIC APERTURE RADAR BASED ON FRACTIONAL FOURIER TRANSFORM WITH APPLICATION TO FOLIAGE PENETRATION

BY

GHAZAL ALI BA KHADHER

A Thesis Presented to the
DEANSHIP OF GRADUATE STUDIES

KING FAHD UNIVERSITY OF PETROLEUM & MINERALS

DHAHRAN, SAUDI ARABIA

In Partial Fulfillment of the
Requirements for the Degree of

MASTER OF SCIENCE

In

TELECOMMUNICATION ENGINEERING

NOVEMBER 2016

KING FAHD UNIVERSITY OF PETROLEUM & MINERALS

DHAHRAN- 31261, SAUDI ARABIA

DEANSHIP OF GRADUATE STUDIES

This thesis, written by **Ghazal Ali Ba khadher** under the direction his thesis advisor and approved by his thesis committee, has been presented and accepted by the Dean of Graduate Studies, in partial fulfillment of the requirements for the degree of **MASTER OF SCIENCE IN TELECOMMUNICATION ENGINEERING**.

Dr. Abdelmalek Zidouri
(Advisor)

Dr. Ali Al-Shaikhi

Department Chairman

Dr. Azzedine Zerguine
(Member)

Dr. Salam A. Zummo
Dean of Graduate Studies

Dr. Ali Muqaibel
(Member)

24/1/17

Date

This work is dedicated to my beloved parents, Ali Salim Ba khadher, Umm Ayman & my wife.

ACKNOWLEDGMENTS

Most importantly, I would like to express my gratitude to Allah for providing me the strength and the blessings to finish my thesis. I thank him for the chance to get the scholarship to pursue my master degree at KFUPM that paved the way for me into the world of research.

My deepest gratitude is to my supervisor, Dr. Abdelmalek Zidouri. I have been amazingly lucky to have an advisor who gave me the freedom to explore on my own and simultaneously the instructions to get back when my steps faltered. I would appreciate and thank the members of the committee that I worked with: Dr. Ali Muqaibel and Prof. Azzedine Zerguine for their help, comments, recommendation, and constructive criticisms in order to produce a quality work.

Finally, I am grateful for the support that I have received from my family, my parents to my brothers and sister, during the time when I was preparing this work and in my general life.

TABLE OF CONTENTS

LIST OF TABLES

LIST OF FIGURES

LIST OF ABBREVIATIONS

CP	:	Cyclic Prefix
DRFM	:	Digital Radio Frequency Memory
DFrFT	:	Discrete Fractional Fourier Transform
DFT	:	Discrete Fourier Transform
ECM	:	Electromagnetic Compatibility
eFrCSA	:	Enhanced Fractional Chirp Scaling Algorithm
FCC	:	Federal Communication Commissions
FFT	:	Fast Fourier Transform
FM-CW	:	Frequency Modulated Continuous Wave
FOPEN	:	Foliage Penetration
FrFT	:	Fractional Fourier Transform
FrRDA	:	FrFT-Based-Range-Doppler Algorithm
GRL	:	Generalized Likelihood Transform
IDFT	:	Inverse Discrete Fourier Transform
IFFT	:	Inverse Fast Fourier Transform

IFrFT	:	Inverse Fractional Fourier Transform
IRCI	:	Inter-Range-Cell-Interference
ISI	:	Intersymbol Interference
LFM	:	Linear Frequency Modulated
LGA	:	Low-Grazing Angle
MIMO	:	Multiple Input Multiple Output
NASA	:	National Aeronautics and Space Administration
PAPR	:	Peak to Average Power Ratio
PN	:	Pseudorandom Noise
PRF	:	Pulse Repetition Frequency
PRI	:	Pulse Repetition Interval
RCMC	:	Range Cell Migration Correction
RCS	:	Radar Cross Section
SAR	:	Synthetic Aperture Radar
UHF	:	Ultra High Frequency

ABSTRACT

Full Name : Ghazal Ali Ba khadher

Thesis Title : UWB OFDM Synthetic Aperture Radar Based On Fractional Fourier Transform With Application To Foliage Penetration

Major Field : Telecommunication Engineering

Date of Degree : November 2016

In this thesis, two different parts have been investigated. First of all, Ultra Wideband (UWB) Orthogonal Frequency Division Multiplexing (OFDM) with sufficient Cyclic Prefix (CP) has been investigated for the application of synthetic aperture radar (SAR) for foliage penetration (FOPEN). The model used for the incorporation of the foliage penetration is the one developed at the University of Nebraska-Lincoln. It is noticed that the foliage distorts the image of single point target due to the fluctuation of the side lobes of the normalized range profile and the normalized azimuth profile compared to synthetic aperture radar without FOPEN. The fluctuation of CP-based OFDM signal has been compared with the random noise signal. It is observed through the integrated side lobe ratio (ISLR) and the peak side lobe ratio (PSLR) that the CP-based OFDM signal has the lower fluctuation of the side lobes along the range direction compared to the random noise signal, while in the azimuth direction is the same. Finally, an arrangement of a few single point targets has been considered to investigate the capability of UWB CP-based OFDM SAR for FOPEN in the scenario where is an extended target, tank, on the ground.

Secondly, OFDM signal based on the Fractional Fourier Transform (FrFT) rather than the Discrete Fourier Transform (DFT) which has received much attention in the

communication system has been adopted for the application of SAR. Reconstruction of the range profile has been developed and then combined with the processing on the flight path as in the range-Doppler algorithm. Then, a point target and an extended target have been considered to show the capability of this signal with the analysis of the side lobes of the point target through the normalized range profile and the normalized azimuth profile. It is found that the side lobes along the range direction are lower compared to the side lobes of the DFT-based OFDM signal.

ملخص الرسالة

الاسم الكامل: غزال علي سالم بخضر

عنوان الرسالة: الرادار ذو الفتحة الاصطناعية (SAR) باستخدام الترادات المتعامدة فائقة العرض على اساس تحويل فوريه الكسري مع التطبيق في اختراق الاشجار

التخصص: هندسة الاتصالات

تاريخ الدرجة العلمية: نوفمبر ٢٠١٦

في هذة الاطروحة , تمت دراسة جزئين مختلفين. أولا, تم التحقق من أشارة مضاعفة الانفسام الترددي المتعامد فائقة العرض مع البادئة الدورية لتطبيق الرادار ذو الفتحة الصناعية في اختراق الاشجار. النموذج المستخدم لدمج تأثير أوراق الشجر هو البرنامج الذي تم تطويره في جامعة نبراسكا. وتم ملاحظة أن أوراق الشجر تعمل على تشوية صورة الهدف ذو النقطة الواحدة بسب تذبذب الفصوص الجانبية من ملف النطاق المطبع وملف السمت المطبع للرادار ذو الفتحة الاصطناعية عند أختراق الاشجار مقارنة بالرادار ذو الفتحة الاصطناعية. وقد تم مقارنة تذبذب أشارة مضاعفة الانقسام الترددي المتعامد فائقة العرض مع البادئة الدورية مع أشارة الضوضاء العشوائية فائقة العرض. لوحظ من خلال نسبة الفص الجانبي المتكاملة ونسبة ذروة الفص الجانبي أن اشارة مضاعفة الانقسام الترردي المتعامد لديها أقل تذبذب للفصوص الجانبية على ملف النطاق مقارنة مع أشارة الضوضاء العشوائية, بينما على ملف السمت لديهم نفس التبذبذب. أخيرا تم ترتيب مجموعة من الاهداف ذو النقطة الواحدة للتحقق من قدرة أشارة مضاعفة الانقسام الترددي المتعامد فائقة العرض للرادار ذو الفتحة الاصطناعية في أختراق الشجر عندما يكون هناك هدف ممتد مثل دبابة موجودة على الارض من أجل تصويرها كهدف. ثانيا, أستخدام أشارة مضاعفة الانقسام الترددي المتعامد على أساس تحويل فوريه (Fourier) الكسري بدلا من تحويل (Fourier) السريع الذي حصل على أهتمام كبير في نظام الاتصالات لتطبيق الرادار ذو الفتحة الاصطناعية . وقد تم بناء ملف النطاق التي تم دمجة مع المعالجة على مسار الرحلة كما هو الحال في خوارزمية نطاق دوبلر. ثم تم اعتبار الهدف ذو النقطة الواحدة والهدف الممتد على شكل دبابة لإظهار قدرة هذه الإشارة مع تحليل الفصوص الجانبية للهدف ذو النقطة الواحدة من خلال أيجاد ملف النطاق المطبع وملف السمت المطبع. وتبين أن الفصوص

الجانبية على طول ملف النطاق أقل من الفصوص الجانبية لاشارة مضاعفة الانقسام الترددي المتعامد على أساس تحويل فوريه المنفصل (DFT).

CHAPTER 1

INTRODUCTION

1.1 Introduction

Synthetic aperture radar (SAR) is considered as one of the most state-of-the-art engineering inventions of the twentieth century [1]. SAR is a radar system for remote sensing techniques that can produce maps with a high resolution of remote targets on a terrain or more generally on a scene, a planet and so forth, in a two-dimensional spatial domain of range and azimuth direction [1]. In 1953, Carl Wiley realized that if the movement of a platform on which the radar is placed, is utilized to collect the echo signal along the flight path, the cross-range direction, then the Doppler spectrum of the received signal can be utilized to synthesize a much longer aperture. Therefore, the adjacent objects along the azimuth direction will be easily resolved [2].

The first use for SAR to form images was in 1953 when a C-46 aircraft was utilized to map a part of Key West, Florida [3]. The researchers at National Aeronautics and Space Administration (NASA) developed the first onboard satellite SAR system and put on Seasat, the first civilian spaceborne SAR, in 1978. This remarkably launched satellite by NASA has opened the way for collecting data for applications in oceanography.

Besides the use of SAR for the applications of surveillance such as the detection of the territories of the opponents, airplanes, tanks, and buildings, it is also used for many other applications [5]. In geology, some air and space vehicles have been utilized to monitor the earth's surface motion to assist us better grasp volcanoes and earthquakes in order to predict them early. In oceanography, SAR systems can be used as a tool to map winds, features of the ocean surface, ocean currents, the thickness of sea ice, and coastal processes accurately. In agricultural, SAR applications are focused on assessing the health of crops and forests. In ecology, SAR systems are being used for the classification of land cover and measurements of biomass. SAR for environmental science application has been used for classification of the forest, monitoring of hazards, a spill of oil, and the observing of squatters who live in cities. SAR systems can also be used for finding oil or other natural resources. SAR-based systems have been used for the detection and the imaging of the objects on the subsurface ranging from archeological to mines substances.

The range profile reconstruction (RPR) of SAR is the 1-dimesional image of the scene to be resolved along the range direction. To achieve long distance imaging, the duration of the transmitted signal must be long enough to carry enough energy, while for the requirements of high-resolution the bandwidth of the transmitted signal must be high. To solve the contradiction between the duration and the bandwidth of the signal, coding of the transmitted pulse either using frequency or phase modulation (i.e. linear frequency modulated (LFM) and step frequency signal) in order to have bandwidth B which is greater compared to that of an uncoded pulse where the duration of time is the same. Then at the receiver side, pulse compression techniques such as the matched filter or correlation are used to get narrow pulse response [6]. However, the interference that

arises between the adjacent cells along the range direction is termed as the "inter-range-cell interference" (IRCI) due to the ambiguity function's side lobes leads to the blurring of the target's image

Orthogonal Frequency Division Multiplexing (OFDM) system with sufficient Cyclic prefix (CP) in a communication system has the ability to eliminate the intersymbol interference (ISI) that arises due to the multipath phenomenon that happens in a communication system. Zhang et al 2015 [7] adopted the use of OFDM system with sufficient CP for SAR application in order to mitigate the IRCI in SAR. The swath width, the strip of the Earth's surface from which data are collected by a side-looking airborne radar, of the radar is divided into *M range* cells. Each range cell considered as one-path as in communication. Then in each OFDM block a guard interval with length *M-1*, excluding the nearest range cell, is added to each OFDM block in a way such that the *M* range cells have free IRCI.

OFDM SAR imaging with sufficient CP is still not yet utilized for application of SAR foliage penetration (FOPEN). Therefore, our aim in this thesis is to investigate Ultra Wideband (UWB) CP-based OFDM SAR for FOPEN and shed the light on the side lobes fluctuation due to the effect of the foliage. Finally, OFDM signal by replacing the discrete Fourier transform with the fractional Fourier transform (FrFT) for SAR application will be investigated.

1.2 Thesis Organization

The first part, Chapter 1, of this thesis is a preface to highlight the concept of SAR and it is an application in many different fields. The remaining part of the thesis will be

organized as the following. Chapter 2 provides the concept of SAR followed by the undesired phenomena and OFDM system. Furthermore, literature review details what have been achieved so far in SAR FOPEN, OFDM radar, and OFDM SAR, range ambiguity suppression, CP-OFDM SAR, and FrFT. Chapter 3 deals with the use of OFDM signal with the addition of sufficient CP to construct the image of SAR in a way that the IRCI is eliminated. Furthermore, the performance of CP-based OFDM SAR is compared with different signals for SAR application such as LFM, OFDM without CP waveform and a random noise waveform. Chapter 4 utilizes UWB CP-based OFDM SAR for foliage penetration. Chapter 5 investigates the use of the FrFT-OFDM system for SAR for a single point target and extended target with the shape of the tank. Last but not least, chapter 6 summarizes what have been concluded from the work as well as the future work.

1.3 Thesis Contribution

Nowadays, OFDM signal for SAR has witnessed a lot of attention and it is still growing on in the field of the radar imaging. Having gone through the literature review, the following areas in OFDM signal for SAR has been found and our contributions mainly focus on the following items:

1. UWB CP-based OFDM SAR for the application of FOPEN.

2. OFDM signal based on FrFT rather than the Discrete Fourier Transform (DFT) for the application of SAR.

CHAPTER 2

TECHNICAL BACKGROUND AND LITERATURE REVIEW

2.1 Introduction

In this chapter, some of the technical backgrounds of SAR concepts that the reader will encounter during this study will be briefly explained. Furthermore, the literature review will cover what have been done so far in the field of SAR.

2.2 Technical Background

This section will introduce the technical backgrounds of SAR and OFDM. First of all, the concept of SAR will be introduced. Secondly, some of the terminologies that are used in radar will be mentioned briefly. Furthermore, range migration which is phenomena that happen in SAR will be briefly described. Last but not least, the concept of OFDM and UWB technology will be elaborated briefly.

2.2.1 Principle of Synthetic Aperture Radar

Radar is a system that used for the detection of objects by sending an electromagnetic signal toward the objects and receiving an echo, the reflected signal, in order to determine the range, the altitude, the speed, or the direction of the targets. The range is the distance between the target and the radar which can be obtained as the following:

$$R = \frac{1}{2}ct \tag{2.1}$$

where t is the round trip propagation time and c is the speed of light.

There are two different types of radars. the passive radar where the receiver takes the advantage of the reflections of sources of illumination in the environment such as wireless fidelity, and commercial broadcast to process them in order to detect and track the targets. The second one is the active radar which has dedicated transmitter in order to transmit an electromagnetic signal toward the target. Then at the receiver, the reflections from the object to be detected or imaged are processed. The latter one can be also divided into two different types based on the aperture of the antenna, (i.e. physical or synthetic), Real Aperture Radar and SAR [8].

Real Aperture Radar or non-coherent radar is one of the active radars which are controlled by the physical length of the antenna, while SAR utilizes the motion of airplane or satellite that carries radar to illuminate the scene by transmitting pulses and record the reflections during the time of flight. On the board or later, the combined reflections from all the signals are processed coherently, in amplitude and phase, to create what we call the "synthetic aperture" in order to get the image of the scene with high resolution. For illustration, consider Figure 2.1, where there is side-looking of the stripmap SAR geometry with three positions of the radar, *A, B, C,* and point target on the ground with the coordinate $(x_m, y_m, 0)$. The radar at each position, *A, B, C,* transmits and record the echo reflected from the target coherently. Finally, the recorded data which is known as the raw radar data are processed to get the final image.

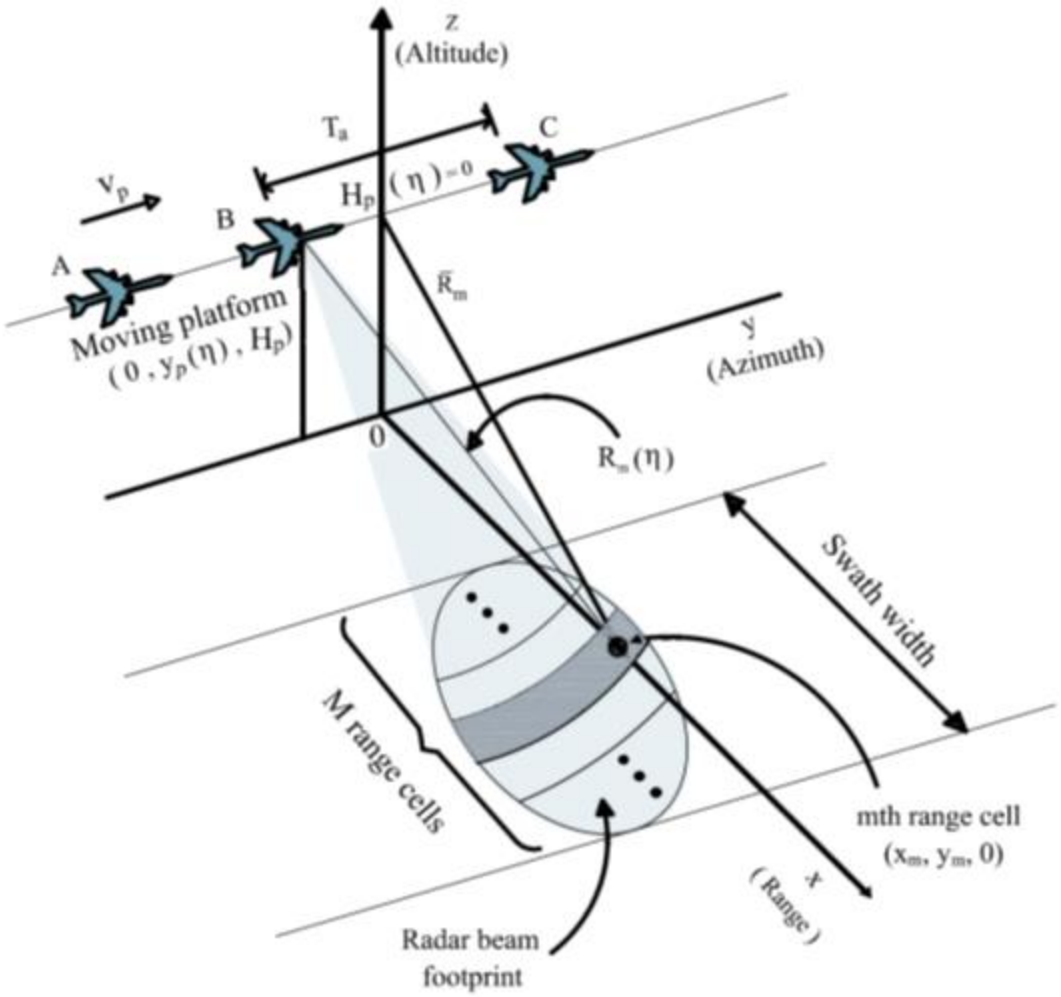

Figure 2.1 Geometry of stripmap SAR

2.2.2 Radar Terminology

The following parameters are crucial in SAR system design. Radar placed on an airplane or a satellite is used for the measurement of SAR and as such, we have to take some parameters into consideration.

Pulse Repetition Frequency

Pulse repetition frequency (PRF) is known as the number of transmitting/ receiving the pulsed radar cycles complete in one second which is measured in Hertz (cycles per

second) as shown in Figure 2.2 [9]. The PRF can be related to the pulse repetition time (PRI) as the following:

$$PRF = \frac{1}{PRI} \tag{2.2}$$

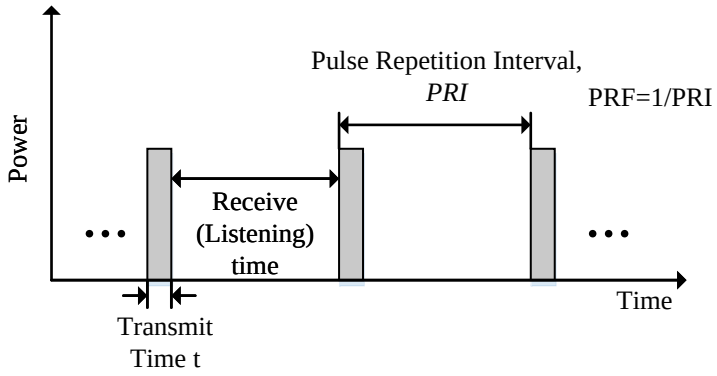

Figure 2.2 Pulse radar waveform [9]

Range Sampling

Once the echo is received at the receiver, A/D converter is used to sample the signal at discrete time intervals. Figure 2.3 shows a sequence of two transmit pulses with its hypothetical target echo signal [9]. The discrete time samples represent a different range increment, called range bin or range cell. The location of the target in Figure 2.3 is at a range corresponding to range sample number five.

Range Migration Correction

Range migration is a phenomenon that happens in SAR because of the variation of the slant ranges between the radar and the target as in [5]. In other words, the distance between the radar and the target has hyperbola trend that makes the distance migrate from cell to another cell while the radar is moving to synthesize long aperture.

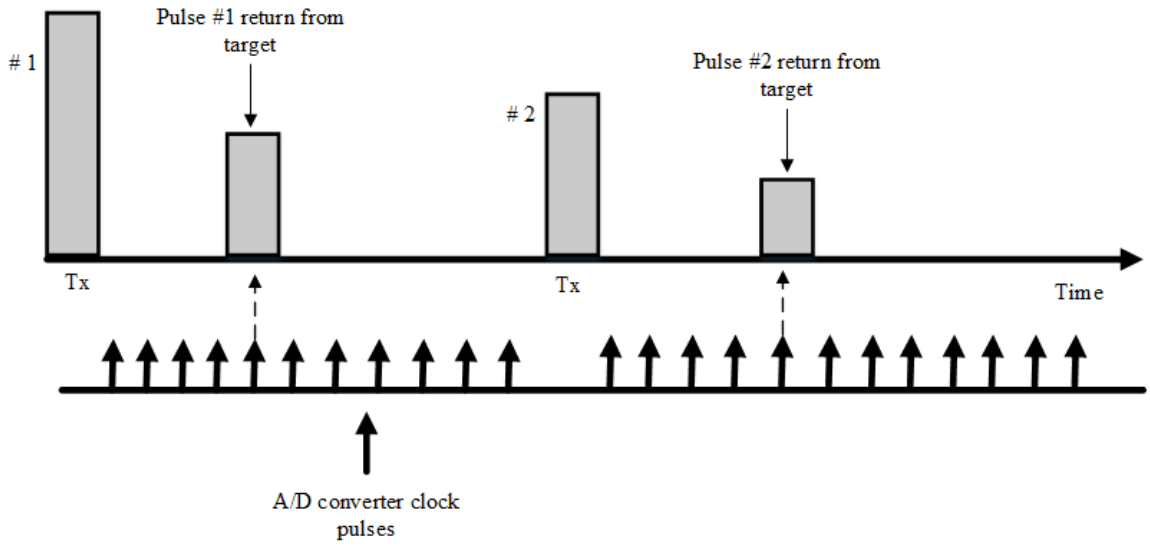

Figure 2.3 Pulse radar waveform showing ADC clock pulses

To help better understand this phenomenon, consider Figure 2.4, where the concept of the migration in the range for single point target under SAR is illustrated. The figure shows the relationship between the slant range $R\ (u)$ as function of the radar position u along the flight path. The range cell lines are represented by the vertical dash lines, while the azimuth or radar positions are represented by the horizontal dash lines. The two points $R1$ and $R3$ are the start and the end of the slant range points during the interval of time the radar illuminating the single point scatterer. The slant range point $R2$ is the point at which the center of the radar beam is on the single point scatterer while the corresponding radar positions for the slant range points $R1$, $R2$ and $R3$ are u_1,u_2 and u_3 respectively. The total range migration is the difference between R_1 and R_3 . Therefore, in this example the range migrates from range cell $R1$ to range cell $R3$, then stops at range cell R3 making the total range migration is 5 range cells [5]. As a result, range cell migration correction (RCMC) is used to mitigate this undesired phenomenon.

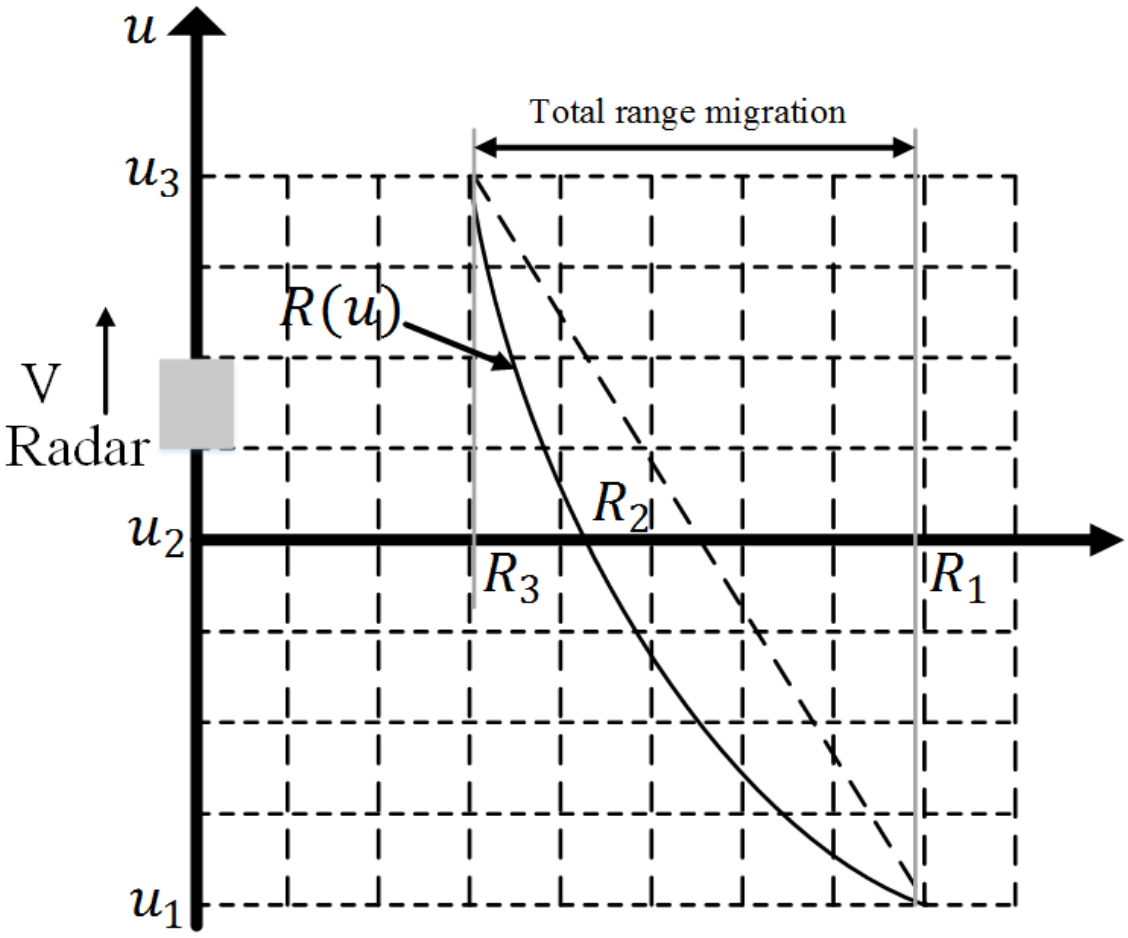

Figure 2.4 Single target trajectory of SAR system

Range Ambiguity

In radar systems, the finding of the target's distance is linked to the amount of time needed for the transmitted signal to travel toward the target and reflect back from the target toward the receiver of the radar. However, for the purpose of measuring the range of the target unambiguously, the transmitter of the radar should wait sufficient time in a way such that the reflected signal from the object received before the transmission of the next pulse otherwise uncertainty (ambiguity) will arise and it will affect the measurement of the target's range. This phenomenon is known as the range ambiguity. To help better

understand the mechanism of this phenomenon, consider Figure 2.5 where the radar transmits two pulses one after the other $s_a(t)$ and $s_b(t)$ respectively. The delayed reflected signal (echo) of the ambiguous range transmitted by the first pulse $s_a(t)$ received after the radar has already emitted the second pulse $s_b(t)$ as illustrated in Figure 2.5.Therfore, this scenario leads to the result that the reflected signal being ambiguous regarding the pulse $s_a(t)$.

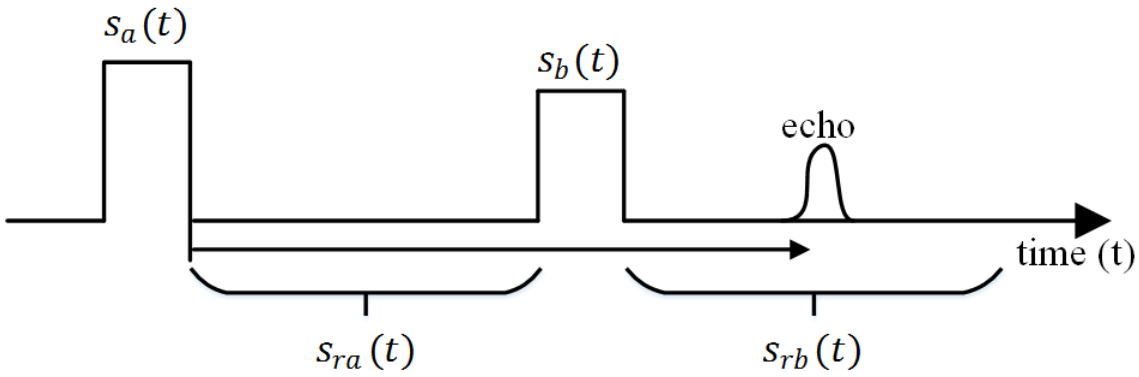

Figure 2.5 Range ambiguity situation

Azimuth Signal Strength and Doppler History

As the platform moves along the flight path, azimuth direction, the target on the ground is illuminated by many hundreds of pulses. The strength of each pulse varies due to the azimuth beam pattern. The azimuth beam pattern for the stripmap case is shown in the top part of Figure 2.6 where three positions of the sensor seen in the slant range plane. At the first position *A*, the target is just getting into the main lobe of the beam. The strength of the received signal is illustrated in the middle part of Figure 2.6. The strength of the signal keeps growing till the target become in the center of the beam, when the sensor is

located at position *B*. After the beam pass the center crossing time, the strength of the signal goes down till the target in the first null of the beam pattern, when the sensor is located at position *C*. from then on, the amount of energy received from the side lobes of beam pattern will be small. Also, the bottom part of Figure 2.6 illustrates the history of the Doppler frequency along the flight path [4].

As the relationship between the Doppler frequency and the target's radial velocity with reference to the radar is related proportionally, when the target is approaching the radar, the Doppler frequency is positive while when the target is moving further away from the radar the Doppler frequency is negative. Therefore, the frequency versus time has negative slope trend as shown in the last part of Figure 2.6.

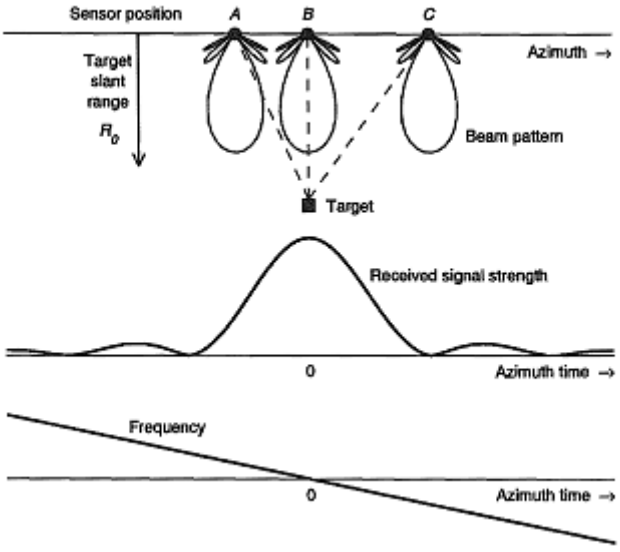

Figure 2.6 Azimuth beam pattern and its effect upon signal strength and Doppler frequency

The strength of the received signal is governed by the azimuth beam pattern. The one-way beam pattern is approximately a sinc function as the following:

$$p_a(\theta) = sinc\left(\frac{0.886\,\theta}{\beta_{bw}}\right) \tag{2.3}$$

where θ is the angle measured form the boresight in the slant range plane, β_{bw} is the azimuth beamwidth, $0.886\lambda/L_a$, and L_a is the antenna length along the azimuth direction. The strength of the received signal is obtained by the square of $p_a(\theta)$ due to the propagation of two-way of the radar energy and it is usually expressed as a function of the azimuth time η.

$$w_a(\eta) = p_a^2[\theta(\eta)] \tag{2.4}$$

2.2.3 Basic Principle of OFDM

OFDM is a multicarrier modulation system as shown in Figure 2.7.

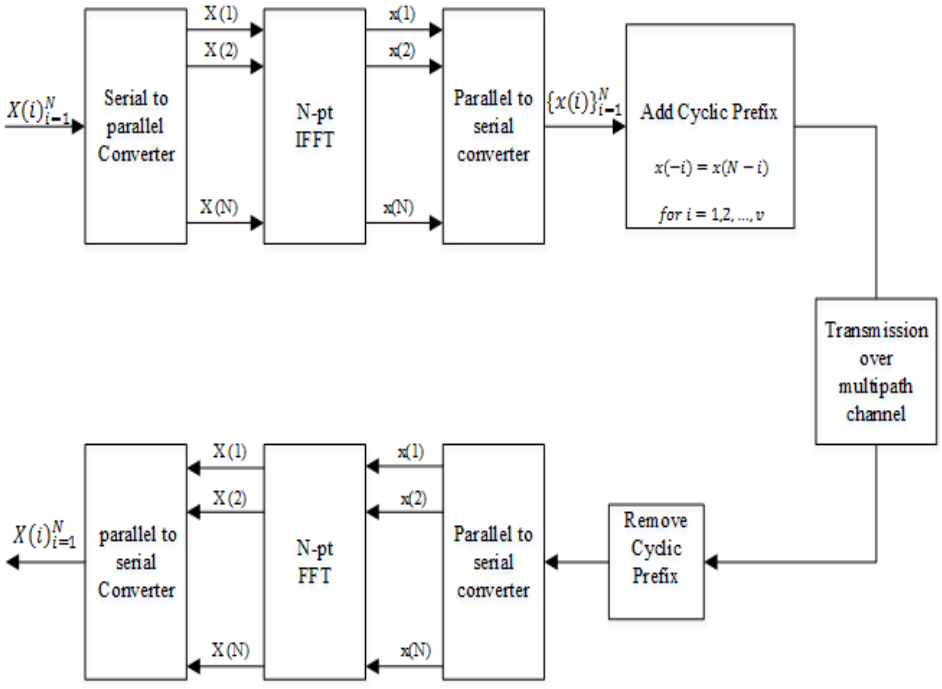

Figure 2.7 OFDM system

The generated data bits is first mapped into symbols by using one of the modulation forms such as QPSK, 16-QAM or 64-QAM to get the symbols $X(i)_{i=1}^{N}$ to be transmitted.

Then these symbols are converted from serial to parallel. After that *N*-point IFFT for the symbols is taken to get $\{x(i)\}_{i=1}^{N}$. The output of IFFT represents a time domain signal in parallel form so the signal is converted into serial using parallel to serial converter block. To eliminate the impact of multipath such as ISI, the last part of the OFDM symbol is copied at the start of the symbol. This part is called the CP and its main purpose is to prevent the different symbols from being overlapping with future and past OFDM symbols. Then The OFDM signal is transmitted over the channel and received at the receiver [10].

At the receiver side, the part of the received signal that has CP is removed. Parallel to serial converter block is used to parallelize the signal in the time-domain. Then, the output is then passed through *N*-point FFT to transform the signal into frequency domain. Finally, parallel to serial is implemented to serialize the signal and demapping it to the corresponding data bits based on the mapping used at the transmitter.

2.2.4 UWB technology

UWB transmission has been defined by the Federal Communication Commissions (FCC) [11] as any signal has fractional bandwidth (B_f) greater than 0.20, or any signal has a bandwidth larger than 500MHz, i.e.

$$B_f \geq 0.2, \text{ or}$$
$$\mathrm{B} > 500\mathrm{MHz} \tag{2.5}$$

where the ratio of the signal bandwidth to the center frequency is defined as the fractional bandwidth and it is expressed as the following:

$$B_f = \frac{B}{f_c} = \frac{(f_H - f_L)}{(f_H + f_L)/2} \tag{2.6}$$

where f_L and f_H are the lowest and the highest transmitted frequencies at the -10 dB emission point, respectively, B is the bandwidth of the signal and f_c is the center frequency. As illustrated in Figure 2.8, it is clear that UWB signals have large fractional bandwidth compared to the conventional radio transmission such as narrowband and wideband systems.

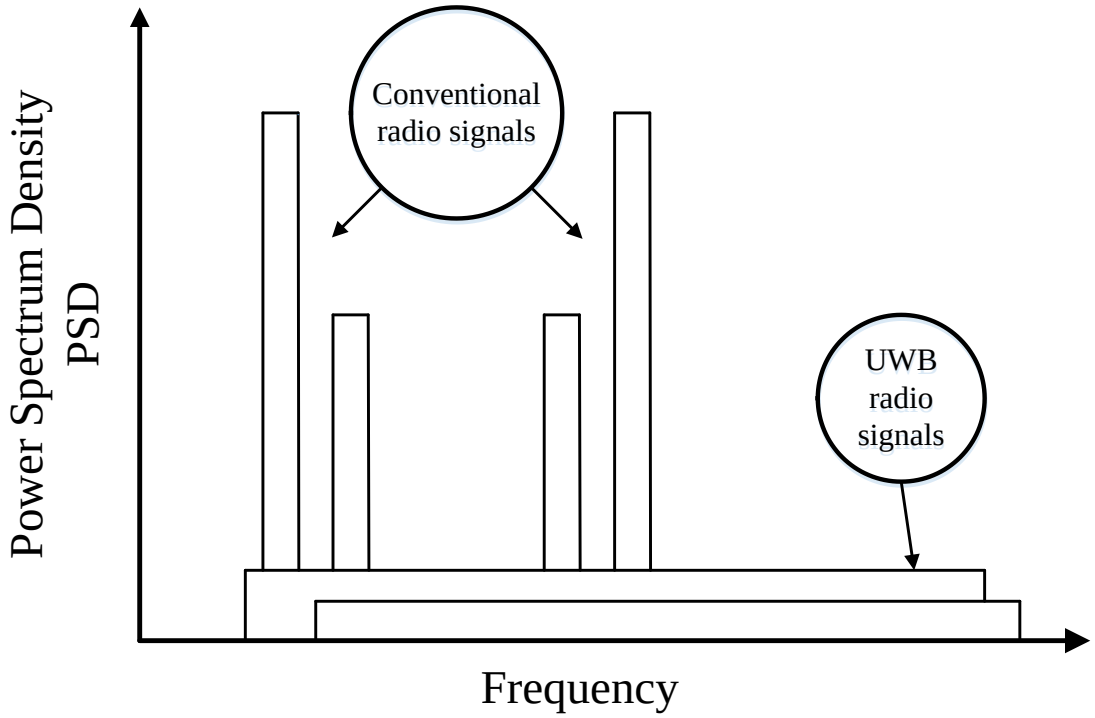

Figure 2.8 The spectrum of the UWB signals versus Conventional signals

2.3 Literature Review

SAR is a remote sensing technique that has the ability to provide high-resolution images regardless of weather conditions and sunlight illumination. This capability of this technology encouraged the researchers to carry out SAR image processing with different transmitted signals. One of these is the LFM signal which is the well-studied SAR signal where the frequency is changed linearly within the pulse [1]. Moreover, stepped frequency (Hop-Frequency) radar where the carrier frequency hops linearly or randomly from subpulse to subpulse has been investigated in [12]. In linear stepped frequency radar, the cells along the range direction are reconstructed by the fast Fourier transform processing, while for the random stepped-frequency radar by the correlation between the reference signal and the received signal. The latter has the ability to suppress the ambiguity in range, enhance covert detection, and decrease the interference from other sensors close to it. On the other hand, the side lobes of the range-Doppler are affected by a noise component. Furthermore, noise radar is a radar technology that uses noise/chaotic/random waveform as a transmitting signal. The echo detection is based on optimal reception and correlation of the transmitted signal and the received noise waveform radar returns. Finally, OFDM signal has been exploited for radar application as in Subsection 2.3.

2.3.1 Synthetic Aperture Radar Foliage Penetration (SAR-FOPEN)

SAR foliage penetration is an imaging of stationary military vehicles which are camouflaged or hidden in forests and tree-lines. Imaging targets under dense foliage have three effects, the attenuation of the incident and backscattered energy, the forming of strong backscatter clutter and the fluctuation of the amplitude and the phase of the foliage

which blur the reconstructed image of the object [13]. The reflections of waves, radar backscatter, from vegetation canopy and forest, have witnessed much attention in the past two decades. Many models of the foliage based on the electromagnetic wave scattering have been developed. These models, based on the biophysical and the geometry of the forest components and operation and observation radar parameters, measure the reflection of wave coefficients and or the average attenuation. Some of these developed typical models are the Michigan microwave canopy scattering model (MIMICS) [14, 15] and the models proposed at the University of Texas at Arlington (UTA) [16, 17].

With the recent advancement in FOPEN-SAR imaging, it is concluded that the amplitude and the phase fluctuations have the most important effect on the SAR-FOPEN. These fluctuations blur the target image. As a result, many experimental and simulation studies for this purpose have been carried out by many researchers.

Sheen, et al [18] conducted an experiment based on ground-based UWB SAR system and calculated the reflection of wave and the characteristics of transmission for foliage. Therefore, a linear model has been developed to delineate mean attenuation of the foliage, the broadening of SAR resolution and the integrated side lobe ratio (ISLR) as a function of the grazing angle, frequency and the biomass of the forest.

Simulation and theoretical studies have been carried out also. A theoretical model has been proposed by Hsu, et al [19] to measure the mean attenuation of the foliage and to calculate the amplitude and the phase fluctuation. The mean attenuation is found from the sum of absorption loss due to the dielectric property of the scatterer and scattering loss due to that wave which is scattering into other directions by the scatterer. The fluctuation

of the amplitude is measured, using the radiative transfer theory, from the bistatic scattering coefficients, while the fluctuation of the phase is found from the fluctuation of the amplitude presuming that the fluctuation of the phase field is uniformly distributed from $-\pi$ to π.

Finally, UHF band UWB random noise SAR for FOPEN with developed statistical-physical transmission model has been studied for the identification of obscured targets with foliage at the University of Nebraska-Lincoln (UNL) [20]. Moreover, the model has been proposed to simplify the simulation instead of the previous models that depend on the electromagnetic principle. Furthermore, the technique of paired echo is used to analyze the foliage obscuring model. The model proposed for the foliage effect represented by transfer function has nonlinear characteristic for both of the phase and the amplitude. The attenuation's mean and the fluctuation of the amplitude considered being the two components of the amplitude characteristics, while the components of the phase characteristics are the linear phase and the fluctuation of the phase. The model also exhibits the dominant observations of foliage transmission experiments. Based on the technique, paired echo, to analyze the pattern of the foliage, the phase fluctuation on the SAR image is very serious than the amplitude fluctuation, while the effect of both them on the SAR image leads to increase the side lobes of the image. The quality of the image of obscured target using a UHF band UWB random noise SAR is similar to UWB stepped frequency radar provided that the former radar has to take sufficient integration of the returned signal for every range cell.

2.3.2 OFDM Radar and OFDM SAR

Nowadays, OFDM has been exploited for radar application. Levanon [21] was the first to introduce OFDM signal for radar application and further investigation was carried out in [22-27]. In [22] closed-form expression for the compression loss, the expected value of the ambiguity function divided by the same function in case of no Doppler, due to the Doppler shift that arises from the target speed has been found for radar using OFDM-coded signal. Furthermore, setting the limit of the compression loss using single pulse is achieved through limiting the speed of the target. Conceptual design of OFDM as a dual system of radar and communication has been studied in [13, 24] where the pulse diversity of this system improves its anti-detection and anti-jamming performance.

A novel approach of range profile reconstruction of OFDM radar based on the modulated symbols developed in [25] regardless of the information transmitted which enable it to be used in parallel for transmitting information. The approach also surpassed the drawbacks of the introduced high side lobes in the radar range profile. The range profile is reconstructed by dividing the received information by the transmitted information. After that, the divided information is transformed into a continuous function in time using the discrete-time Fourier transform. The method also reduces the computational cost by the use of discrete-time Fourier transform instead of the correlation-based technique.

On the other side, the cross-range profile reconstruction of SAR has been achieved by many methods based on the transmitted waveform. The well-known one is LFM where the range-Doppler algorithm is used for focusing the raw data. Furthermore, a modified range-Doppler algorithm for wideband frequency modulated continuous waveform (FMCW) has been proposed [26]. The phase of the signal could be expressed analytically

for the two cases due to the structure of LFM signal, but the phase could be approximated to the analytical expression for the sake of achieving higher efficiency of an algorithm. Zaugg et al [27] proposed generalized frequency domain SAR focusing method for only LFM signal with the aim of introducing uncompleted, more useful method rather than the approaches in the time domain, where the phase approximation errors controlled in order to achieve the desired accuracy. Furthermore, Garmatyuk [28] developed a new approach for the cross-range profile reconstruction with multicarrier OFDM signals. The azimuth components of OFDM SAR signal are separated. Then the phase /Doppler histories of these components are estimated numerically using the least square estimation method. Finally, a matched filter of the estimated phase history is used to construct the cross-range profile.

Detection and tracking of moving target with low-grazing angle have been studied in [29, 30]. In [29], a parametric model for the detection of moving target using multicarrier OFDM radar in an environment where the clutter is present is developed with the use of the generalized likelihood ratio (GLR) test as a detector. Moreover, the asymptotic performance analysis is used to analyze the performance of the detector which paves the way for an approach to optimize the parameters for the next emitted signal to enhance the probability of detection. Tracking of low-grazing angle target using "OFDM MIMO radar with mutual information waveform" design have been developed in [30]. The model accounts for the statistical and realistic physical effects that happen in target tracking scenario with a low-grazing angle (LGA).

2.3.3 Range Ambiguity Suppression

Range ambiguity is an undesired phenomenon that occurs in SAR as a result of the long delayed echo of the transmitted signal. In other words, this problem occurs as the result of the arrival of signal contributed to the transmitted pulse (n) while the radar has already emitted a new pulse (n+1). This long delayed echo degrades the resolution of the image and it appears as a shadow. As a result, range ambiguity attracts the attention of many researchers. A known tradeoff for the solution of range ambiguity in SAR is increasing or decreasing the PRI. Reducing the PRI avoids the ambiguity in the range. However, the azimuth ambiguity is increased and vice versa. Based on this contradiction, Mittermayer et al [31] suggested the use of signals alternation, up and down chirp signals, for the suppression of the ambiguity in the range. Furthermore, Riche et al [32] proposed a method to increase the PRF for the sake of avoiding the ambiguity in the range through the use of coded-OFDM radar and claimed that their approach outperforms the alternation of up and down chirp signals. Furthermore, Riche et al [33] where OFDM signals were used to alleviate the cross correlation between each emitted pulse. Also, Riche et al [34] proposed the same idea used in [33] with the adoption of a genetic algorithm for the purpose of coding OFDM signals.

2.3.4 OFDM SAR Imaging with Sufficient Cyclic Prefix

OFDM with sufficient CP has the ability to eliminate ISI that arises in communication system due to multipath. Likewise in SAR, the ambiguity function's side lobes are the reason behind the interference between the cells along the range direction, which is known as IRCI. As a result, Zhang et al [7] proposed OFDM signal with sufficient CP for SAR application to eliminate the IRCI problem in order to get high range resolution SAR

images. However, the CP length is nearly equal to the number of range cells in a swath, while the number of the subcarriers must be greater than the length of the CP. Therefore, this makes the length of the OFDM signal almost twice the number of cells along the range direction. As a result of these drawbacks, Zhang et al [35] developed an algorithm to generate a CP-OFDM signal with an arbitrary pulse length independent of the swath width and achieved zero side lobes. Furthermore, the peak to average power ratio (PAPR) issue in CP-OFDM is reduced using a method called clipping and filtering.

2.3.5 Fractional Fourier Transform

FrFT, which is a generalization method of Fourier transform, has been used for applications in radar systems, detection of chirp signals, pattern recognition, and processing of SAR images [36]. The "range-Doppler algorithm" is a classical approach that continues to receive interest to focus the raw data at the receiver. Both of the range and the azimuth involve the use of Fourier transform to compress the data in each direction separately using the matched filter. Clemente et al [36, 37] used the FrFT with appropriate fractional domain for chirp signal instead of the ordinary Fourier transform to do the compression in the range and in the azimuth using the "range-Doppler algorithm" and the "chirp scaling algorithm" for the focusing of SAR images and claimed that it has better ability in focusing the SAR image than the Fourier transform. Furthermore, Clemente et al [38] addressed the problem of shift variant that arose due to the adoption of FrFT which leads into modulation effect that cannot be reduced from the received signal. This problem is resolved by the introducing of a new "FrFT-based Range-Doppler algorithm" (FrRDA) and "enhanced Fractional chirp scaling algorithm" (eFrCSA). Finally, El-Mashed et al [39] extended the work of using FrFT by derived closed form

expressions for the azimuth and the range compression. Last but not least, it was the first paper to introduce the effect of the channel into SAR with the use of regularized deconvolution technique in order to enhance the image in the presence of the channel.

2.4 Research Motivation

According to the above literature review, OFDM for SAR has witnessed a lot of attention in order to eliminate the IRCI and the FrFT in SAR. However, based on the literature review, we concluded the following.

- No work has been done for SAR foliage penetration using OFDM with sufficient CP.

- The use of the FrFT instead of the discrete Fourier transform in OFDM system for SAR application has not yet been investigated.

So the main contribution of this study is to investigate the above mention items.

2.5 Chapter Summary

This chapter shed light on the principle of SAR, the needed fundamentals in order to better understand the subsequent chapters and the literature review that paved the way for our contribution. First of all, the concepts of SAR have been elaborated briefly followed by some of the terminology and the phenomena that happen in SAR. Furthermore, the concept of OFDM system that will be utilized in the coming chapters for the application in SAR was addressed. Last but not least, the literature review that provided us with what have been done in SAR regarding the types of the transmitted signal, SAR FOPEN, OFDM radar and OFDM SAR, range ambiguity suppression` and the use of FrFT. The next chapter will illustrate the use of OFDM with sufficient CP for SAR application compared with the already existed one such as LFM, conventional OFDM waveform, and a random noise waveform.

CHAPTER 3

OFDM SYNTHETIC APERTURE RADAR WITH SUFFICIENT CYCLIC PREFIX

3.1 Introduction

The type of the signal for SAR and the reconstruction of range profile of the scene are one of the important factors in order to achieve high resolution. OFDM signal has been intensively utilized in a communication system to eliminate the ISI that arises due to the multipath using CP. As a result, Zhang et al [7] took the advantage of this property with suitable modification to mitigate the IRCI in radar. This chapter deals with this in depth and the comparison with other different signals such as LFM waveform, random noise pulse and conventional OFDM signal with their algorithms to reconstruct the image of the target.

3.2 CP-based OFDM Range Profile Reconstruction

In this section, the approach of RPR is illustrated. First of all, we describe the geometric model followed by the signal model. Moreover, the range compression, as well as the azimuth reconstruction, is explained. Finally, the constraints on the number of subcarriers are discussed.

3.2.1 Monostatic SAR stripmap geometry

Depending on the geometry of monostatic stripmap SAR in Figure 3.1, the radar is placed on an airplane that is moving along the flight path to get the target's image on the ground by sending signals towards the target. The received signals of the target along the

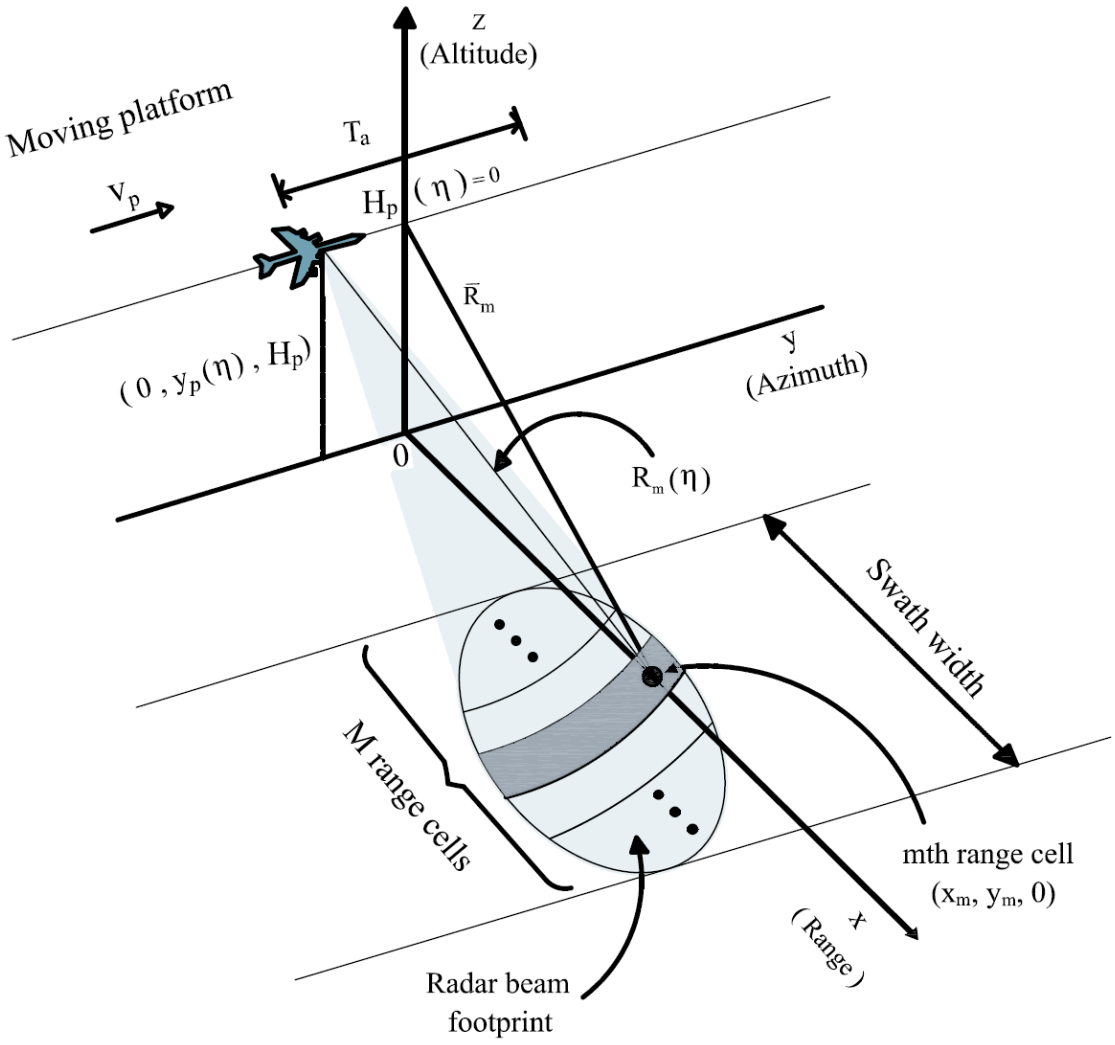

Figure 3.1 Geometry of monostatic stripmap SAR

azimuth direction constructs a matrix with the two-dimensional spatial domain, the range and the azimuth, which is called the raw radar data. Our aim is to focus or to process this

data to form the image of the target. Furthermore, the transmitted and the received signal will be OFDM with sufficient CP because of the advantages of using OFDM with sufficient CP to eliminate ISI in communication and IRCI in SAR. The model illustrated in Figure 3.1 is adapted from the work by Zhang et al [7].

The coordinates of the radar platform along the flight path instantaneously are $(0, y_p(\eta), H_p)$ where the time at which the radar transmit signal along the flight path is η , H_p is the radar platform's height, T_a is defined as the time extent along the flight path over which the target on the ground lies in the antenna beam, synthetic aperture time. Furthermore, the platform's velocity is v_p and $R_m(\eta)$ is the distance for waveform to travel from the radar to the target in the m^{th} range cell with the coordinate $(x_m, y_m, 0)$. The minimum distance is $\bar{R}_m$, the range of closet approach. Finally, the projected beam of the radar antenna onto an area of the ground is known as the radar beam footprint.

3.2.2 OFDM Transmit/Receive Signal model

Suppose that there is an OFDM signal with Bandwidth equal to B Hz distributed between N subcarriers separated by $\Delta f = \frac{B}{N} = 1/T$. Furthermore, assume that we have N symbols, $\boldsymbol{X} = [X_0, X_1, \dots, X_{N-1}]^T$ to be transmitted over the subcarriers. Then the time domain signal is obtained by the IFFT of the vector $\boldsymbol{X}$. Therefore, the OFDM signal will be represented as the following:

$$s(t) = \frac{1}{\sqrt{N}} \sum_{k=0}^{N-1} X_k exp\{j2\pi k\Delta f t\}, \quad t \in [0, T + T_{GI}] \tag{3.1}$$

where t is the length of the OFDM signal that consists of two parts, The time duration of the OFDM signal without the CP is T and the length of the CP is T_{GI}.

For $T = NT_s$ and $T_{GI} = (M-1)T_s$ where $T_s = \frac{1}{B}$ is the sampling frequency. After sampling at $t = iT_s$, (3.1) can be represented as the following:

$$s_i = s(iT_s) = \frac{1}{\sqrt{N}} \sum_{k=0}^{N-1} X_k exp\left\{\frac{j2\pi ki}{N}\right\}, \qquad i = 0,1, \dots, N+M-2 \tag{3.2}$$

and $s_i = 0$ if $i < 0$ or $i > N + M - 2$.

Since the transmitted sequence is prefixed by CP. The transmitted sequence is constructed as the following:

$$\tilde{s} = [s_0, s_1, \dots, s_{N+M-2}]^T, \text{ where } [s_0, \dots, s_{N+M-2}]^T = [s_N, \dots, s_{N+M-2}]^T$$

Once the signal received and demodulated using the quadrature demodulator to the baseband, the received echo from fixed point target lies in the m^{th} cell along the range direction can be represented in terms of the time along the flight path, slow time η, and the fast time t as the following:

$$\begin{aligned} z_m(t,\eta) = \sigma_m \varepsilon_a(\eta) exp\left\{-j4\pi f_c \frac{R_m(\eta)}{c}\right\} \\ \times \frac{1}{\sqrt{N}} \sum_{k=0}^{N-1} X_k exp\left\{\frac{j2\pi k}{T}\left[t - \frac{2R_m(\eta)}{c}\right]\right\} \\ + \omega(t,\eta),\ t \in \left[\frac{2R_m(\eta)}{c}, \frac{2R_m(\eta)}{c} + T + T_{GI}\right] \end{aligned} \tag{3.3}$$

where $\varepsilon_a(\eta)$ is the azimuth beam that governs the strength of the received signal along the azimuth direction which can be represented as the following:

$$\varepsilon_a(\eta) = p_a^2\big(\theta(\eta)\big) = sinc^2(0.886\,\theta/\beta_{bw}) \tag{3.4}$$

θ is the boresight's angle measured in plane of the slant range, $\beta_{bw} = 0.886\lambda\,/L_a$ is the beamwidth along the azimuth direction, L_a is the antenna's length and σ_m is the radar cross section (RCS) coefficient that arise from the targets that lie in the m^{th} cell along the range direction. c is the light's speed, $\omega(t,\eta)$ represent the noise and the distance, the slant range, between the radar and the target in the m^{th} cell along the range direction located at $(x_m, y_m, 0)$ can be represented as the following:

$$R_m(\eta) = \sqrt{x_m^2 + H_p^2 + \big(y_m - y_p(\eta)\big)^2} = \sqrt{x_m^2 + H_p^2 + v_p^2\eta^2} \tag{3.5}$$

where v_p is the platform's velocity on which the radar is carried. Then the received echo from every cell along the range direction within the swath width can be represented as the following:

$$z(t,\eta) = \sum_m z_m(t,\eta). \tag{3.6}$$

After that, the received signal at the receiver side is sampled with $T_s = \frac{1}{B}$ as the sampling interval and the resolution in the range direction is $\rho_r = \frac{c}{2B}$. Suppose that the swath width R_w of the scene to be imaged is shown in Figure 3.2 which is divided by M-range cells $M = \frac{R_w}{\rho_r}$ so the profile along the range direction can be partitioned into M cells.

The main idea of CP-based OFDM SAR is that the swath width is divided into M cells along the range direction in order to represent all the reflected response of the targets in each of the range cell as one multipath as in communication system. As the multipath in

communication system leads to ISI which is mitigated by the use of OFDM system with sufficient CP, the IRCI that arise in SAR due to the ambiguity function's side lobes are eliminated by the use of OFDM with sufficient CP, $M-1$ length,. Then the receiver side of the SAR is modified (not necessarily matched filter). Also, the number of subcarriers N is at least the number of cells along the range direction in the swath which will be illustrated in Subsection 3.2.3.

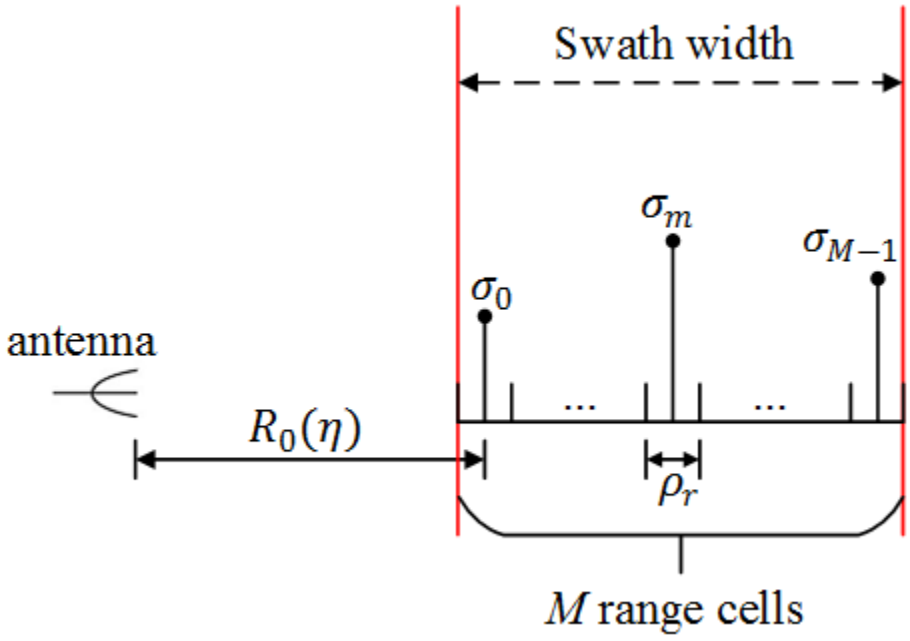

Figure 3.2 Graphical representation of one line along the range direction

As it is known in monostatic SAR that after the transmitted signal, the receiver must wait sufficient time such that all the reflected echo from the targets that lie in the swath width is received before the radar transmit the next pulse which is shown in Figure 3.3.(b). This is represented mathematically by the PRI. Therefore, the length of the PRI should be as the following:

$$T_{PRI} = \frac{1}{PRF} > \left(\frac{2R_w}{c} + T_{GI} + T\right) \tag{3.7}$$

where $R_w = M\rho_r$ is the swath width.

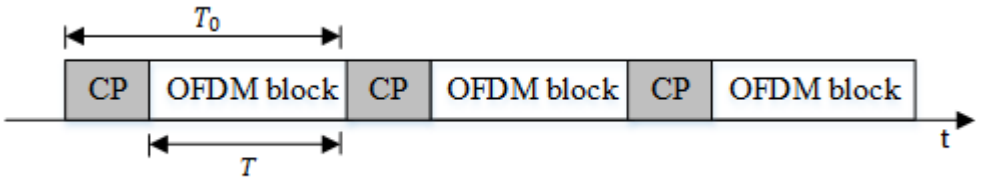

(a)

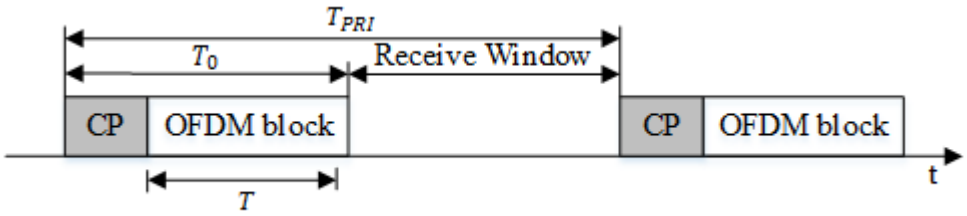

(b)

Figure 3.3 Transmission comparison of OFDM signals in (a) communication system and (b) synthetic aperture radar

From Figure 3.2, we notice that the slant range is $R_m(\eta) = R_0(\eta) + m\rho_r$, therefore, $t - (2R_m(\eta)/c)$ in (3.3) can be written as the following:

$$t - \frac{2R_m(\eta)}{c} = t - \frac{2(R_0(\eta) + m\rho_r)}{c} = t - t_0(\eta) - mT_s \tag{3.8}$$

where $t_0(\eta) = 2R_0(\eta)/c$ is the constant time delay for each azimuth time η independent of m. Suppose that the sampling was done after $t_0(\eta)$ from the first arrival version of the transmitted signal from the transmitter. Therefore, combining (3.3), (3.8) and (3.6), the complex of the received envelope $z(t, \eta)$ can be represented as the discrete time linear convolution of the weighted RCS coefficient with the transmitted sequence as the following:

$$z_i = \sum_{m=0}^{M-1} g_m s_{i-m} + w_i \qquad i = 0,1,\dots,N+2M-3 \qquad (3.9)$$

where

$$g_m = \sigma_m \varepsilon_a(\eta) exp\left\{-j4\pi f_c \frac{R_m(\eta)}{c}\right\} \qquad (3.10)$$

3.2.3 Range Compression

After the signal is received at the receiver side as it is known for OFDM system. The first $M-1$ samples are removed as in communication as well as the final $M-1$ samples are discarded due to the lack of entire M RCS coefficients from all the M cells along the range direction and as result, we obtain the following:

$$z_n = \sum_{m=0}^{M-1} g_m s_{n-m} + w_n\,, \quad n = M-1, M, \dots, N+M-2 \qquad (3.11)$$

This can be represented in matrix form as the following $z = [z_{M-1}, z_M, \dots, z_{N+M-2}]^T$ is

$$\begin{bmatrix} z_{M-1} \\ z_M \\ \vdots \\ z_{N+M-2} \end{bmatrix} = \begin{bmatrix} g_{M-1} & \dots & g_0 & \dots & \dots & 0 & \dots & 0 \\ 0 & g_{M-1} & \dots & g_0 & \dots & 0 & \dots & 0 \\ \vdots & \ddots & \ddots & \ddots & \ddots & \ddots & \ddots & \vdots \\ 0 & \dots & 0 & \dots & \dots & g_{M-1} & \dots & g_0 \end{bmatrix} \times \begin{bmatrix} s_0 \\ \vdots \\ s_{M-1} \\ s_M \\ \vdots \\ s_{N+M-2} \end{bmatrix} + \begin{bmatrix} w_{M-1} \\ w_M \\ \vdots \\ w_{N+M-2} \end{bmatrix} \qquad (3.12)$$

Since the CP$[s_0, \dots, s_{M-1}]^T = [s_N, \dots, s_{N+M-2}]^T$, the vector $\tilde{s} = [s_0, s_1, \dots, s_{N+M-2}]^T$ in (3.12) can be substituted by its tail part s′ and as a result, the matrix representation in (3.12) is corresponding to the following expression as in [7]:

$$\boldsymbol{z} = \boldsymbol{H}\boldsymbol{s}' + \boldsymbol{w} \tag{3.13}$$

where $\boldsymbol{s}' = [s_{M-1}, s_M, \dots, s_{N+M-2}]^T = [s_{M-1}, \dots, s_{N-1}, s_0, \dots, s_{M-2}]^T$,

$\boldsymbol{w} = [w_{M-1}, w_M, \dots, w_{N+M-2}]^{\boldsymbol{T}}$, and $\boldsymbol{H}$ is constructed through the following N by N matrix.

$$\boldsymbol{H} = \begin{bmatrix} g_0 & 0 & \cdots & 0 & g_{M-1} & \cdots & g_1 \\ \vdots & \ddots & \ddots & \vdots & \ddots & \ddots & \vdots \\ g_{M-2} & \cdots & g_{\boldsymbol{0}} & 0 & \cdots & 0 & g_{M-1} \\ g_{M-1} & g_{M-2} & \cdots & g_0 & 0 & \cdots & 0 \\ 0 & \ddots & \ddots & \vdots & \ddots & \ddots & \vdots \\ \vdots & \ddots & g_{M-1} & g_{M-2} & \cdots & g_0 & 0 \\ 0 & \cdots & 0 & g_{M-1} & g_{M-2} & \cdots & g_0 \end{bmatrix} \tag{3.14}$$

Then at the receiver, as it is known in communication system, the OFDM system perform FFT on the vector $\boldsymbol{z}$

$$Z_k = \frac{1}{\sqrt{N}} \sum_{n=0}^{N-1} z_{n+M-1} exp\left\{\frac{-j2\pi kn}{N}\right\}, k = 0, 1, \dots, N-1 \tag{3.15}$$

From (3.13) and (3.14), the preceding Z_k can be written as

$$Z_k = G_k\, S_k' + W_k, k = 0,1, \cdots, N-1 \tag{3.16}$$

where

$$S_k' = \sum_{m=M-1}^{N+M-2} s_m' \, exp\left\{\frac{-j2\pi mk}{N}\right\}, k = 0,1, \cdots, N-1 \tag{3.17}$$

$$W_k = \sum_{m=M-1}^{N+M-2} w_m \, exp\left\{\frac{-j2\pi mk}{N}\right\}, k = 0,1, \cdots, N-1 \tag{3.18}$$

$$G_k = \sum_{m=0}^{M-1} g_m exp\left\{\frac{-j2\pi mk}{N}\right\}, \qquad k = 0,1,\cdots,N-1 \tag{3.19}$$

Therefore the estimation of the weighting RCS coefficient $\hat{G}_k$ is

$$\begin{aligned} \hat{G}_k &= \frac{Z_k}{S'_k} = \frac{Z_k}{S_k exp\left\{\frac{j2\pi k(M-1)}{N}\right\}} \\ &= G_k + \frac{W_k}{S_k} \exp\left\{\frac{-j2\pi k(M-1)}{N}\right\}, k = 0,1,\ldots,N-1 \end{aligned} \tag{3.20}$$

It can be noticed from (3.20) that if S_k is small, the noise will be enhanced. Therefore, the optimal selection of S_k should have constant module for all k's.

The vector $\boldsymbol{G} = [G_0, G_1, \ldots, G_{N-1}]^T$ in (3.20) is the *N*-point FFT of $\sqrt{N}\,\psi$, where ψ is the weighting RCS coefficient vector written as

$$\psi = [g_0, g_1, \ldots, g_{M-1}, \ldots, 0, \ldots, 0]^T \tag{3.21}$$

where the last zeros in the tail of equation have a length (*M*-*N*).

Therefore, the estimation of the weighting RCS coefficient g_m can be obtained by performing *N*-IFFT point on the vector $\widehat{\boldsymbol{G}} = \left[\hat{G}_0, \hat{G}_1, \ldots, \hat{G}_{N-1}\right]^T$

$$\hat{g}_m = \frac{1}{\sqrt{N}} \sum_{k=0}^{N-1} \hat{G}_k \, exp\left\{\frac{j2\pi mk}{N}\right\}, m = 0, \ldots, M-1. \tag{3.22}$$

Afterward, the estimation of the weighting RCS coefficients of the M cell along the range direction can be expressed as the following:

$$\hat{g}_m = \sqrt{N}\, g_m + \widetilde{w'}_m\,, \qquad m = 0, \dots, M-1 \tag{3.23}$$

As the operation of IFFT is unitary transform, the variance of the noise in (3.23) is the same as in (3.20). Furthermore, it can be easily noted from (3.23) that the weighting RCS coefficients are completely reconstructed without any IRCI. Moreover, once the weighting RCS coefficients g_m are determined, the RCS coefficients σ_m can be obtained from (3.10) and vice versa as the following:

$$\hat{\sigma}_m = \hat{g}_m exp\left\{j4\pi f_c \frac{R_m(\eta)}{c}\right\} \tag{3.24}$$

3.2.4 Discussion on the Number of Subcarriers

For $N > M$, the final weighting RCS coefficients in the vector ψ are zeros as in (3.21). Taking into account (3.21) and (3.22), it is clear that section of the transmitted sequence of OFDM signal is utilized to estimate the unreal weighting RCS coefficient. Furthermore, when $N = M$, the length of the vector ψ will be from 0 up to $M-1$ which indicates that the sequence of the emitted OFDM signal will be used to estimate the real weighting RCS coefficient. This case as in [7] known as "swath width matched pulse" (SWMP).

Last but not least, when $N < M$, based on (3.10), the vector of the signal $[s_0, \dots, s_{M-1}, s_M, \dots, s_{N+M-2}]^T$ in (3.2) is $\left[s_0, \dots, s_{M-1}, s_M, \dots, s_{(N+M-2)_N}\right]^T$ where $(n)_N$ is the residue of n modulo N. Therefore, the N by N matrix H in (3.13) and (3.14) can be written as

$$\boldsymbol{H} = \begin{bmatrix} \tilde{g}_0 & \tilde{g}_{N-1} & \cdots & \tilde{g}_1 \\ \tilde{g}_1 & \tilde{g}_0 & \cdots & \tilde{g}_2 \\ \vdots & \vdots & \ddots & \vdots \\ \tilde{g}_{N-1} & \tilde{g}_{N-2} & \cdots & \tilde{g}_0 \end{bmatrix} \tag{3.25}$$

where $\tilde{g}_n = \sum_{i:\ 0 \le iN+n \le M-1} g_{iN+n}$, $n = 0, \ldots, N-1$. It is clear that $\tilde{g}_n$ is reconstructed through the addition of weighting RCS coefficients from several cells along the range direction , in other words, each $\tilde{g}_n$ suffers from IRCI. Therefore, this is the reason behind the requirement of the number of subcarriers to be greater than the number of M cells along the range direction as stated in [7].

3.3 Simulation and Performance Discussion

In this section, the simulation of the proposed CP-based OFDM SAR imaging performed. The azimuth processing for the developed CP-based OFDM SAR is similar to the one used as in the range-Doppler algorithm [1] as shown in Figure 3.4. The reference range cell is set as the value placed at the center of the range swath. After that, the RCMC is implemented. Finally, the azimuth compression is implemented by the matched filter. For the sake of comparison, LFM, conventional OFDM and random noise radar signals with the use of the range-Doppler algorithm are being considered as shown in the block diagram of Figure 3.5 and Figure 3.6 respectively. In Figure 3.5, the range profile reconstruction is achieved by the matched filter in the range. Moreover, the range compression for the two other signals, random noise signal, and conventional OFDM signal is illustrated in Figure 3.6.It is accomplished by the correlation between a replica of the transmitted signal and the returned signal, echo, in the time domain. It is clear that

the difference between the three SAR systems is in the range compression, while the other major stages, RCMC, and the azimuth compression are the same.

The parameters for the simulation of a typical SAR system are shown in Table 3.1. The population of the symbols over the CP-based OFDM waveform's subcarriers and the conventional OFDM waveform's subcarriers to be transmitted is considered to be vectors of pseudorandom noise (PN) sequence of values -1 and 1. Last but not the least, the time durations of the other three signals, LFM pulse, random noise pulse, and conventional OFDM pulse are the same like the CP-based OFDM pulse in order to make the transmission energies equal.

Two scenarios have been considered for the target to be imaged. First, a single point target is placed at the center of the swath width. The images of a single point target are shown in Figures 3.7(a), 3.7(b), 3.7(c), and 3.7(d). The results show that the CP-based OFDM SAR's image is better compared to the other three signals. The boundaries of the point target are noticed to be less distorted by the use of CP-based OFDM for SAR imaging. The normalized range profiles of the point spread function are illustrated in Figure 3.8. It can be clearly noticed that the side lobes of the CP-based OFDM SAR are much lower than the side lobes of the other three signals.

Furthermore, an extended target constructed with the arrangement of a few single point targets to produce tank shape and the results show that the CP-based OFDM SAR in Figure 3.7(e) has superior performance compared to the other three SAR imaging methods as shown in Figures 3.7(f), 3.7(g), and 3.7(h).

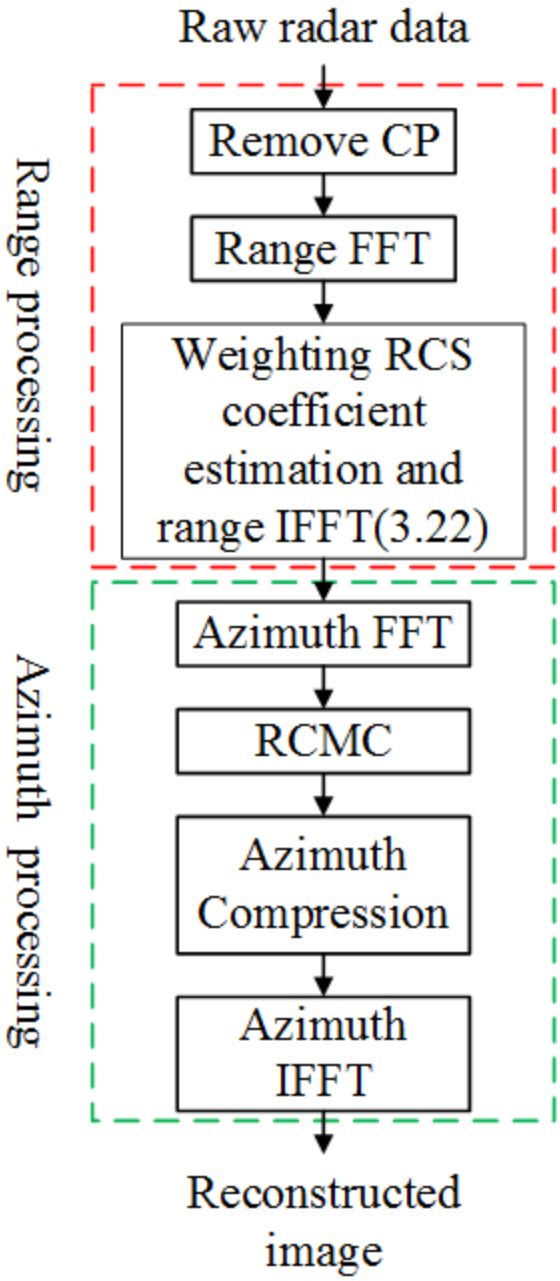

Figure 3.4 Block diagram of CP-based OFDM SAR processing

Table 3-1 List of simulation parameters of CP-based OFDM SAR

Parameters	Symbols	Units	Value
Pulse repetition frequency.	PRF	Hz	800
Bandwidth.	B	MHz	150
The carrier frequency.	f_c	GHz	9
The sampling frequency.	f_s	MHz	150
The antenna length.	L_a	M	1
The synthetic aperture time.	T_a	Sec	1
The speed of the airplane.	v_p	m/s	150
The height of the airplane.	H_p	Km	5
The slant range swath center.	R_c	Km	$5\sqrt{2}$
The number of range cells.	M	-	96
OFDM signal duration without CP.	T	us	3.41
The number of OFDM subcarriers.	N	-	512
The CP length.	CP_{length}	-	95
The duration of CP.	T_{GI}	us	0.63
CP-based OFDM pulse duration.	T_0	us	4.05

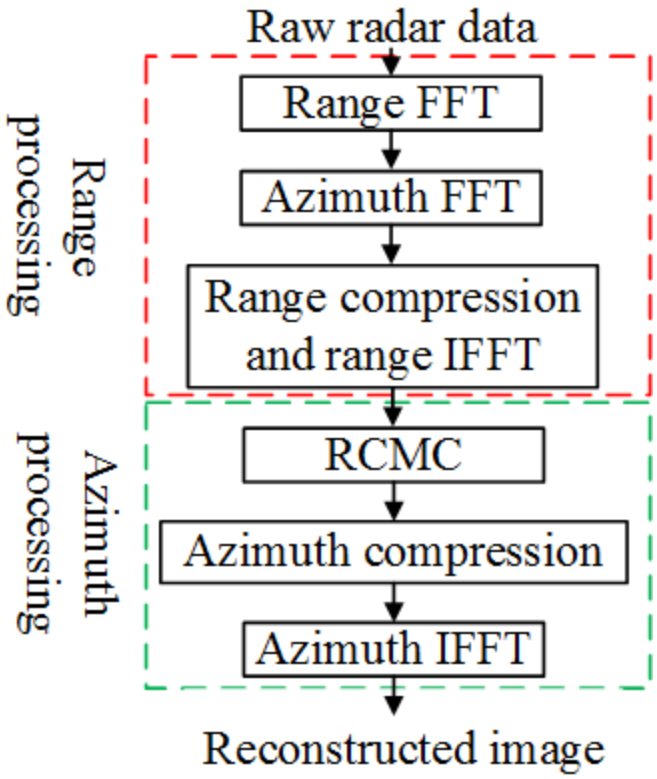

Figure 3.5 Block diagram of LFM SAR processing

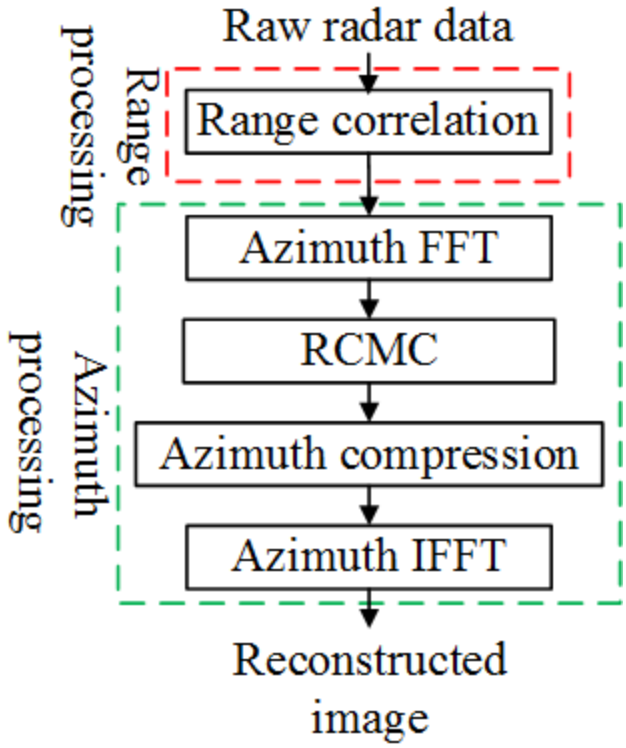

Figure 3.6 Block diagram of random noise and conventional OFDM SAR processing

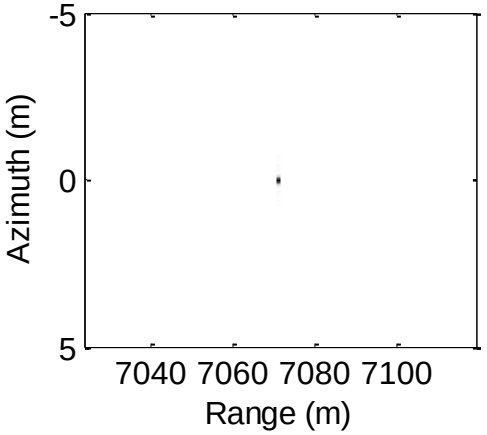
-5
0
5
Azimuth (m)
7040 7060 7080 7100
Range (m)
(a)

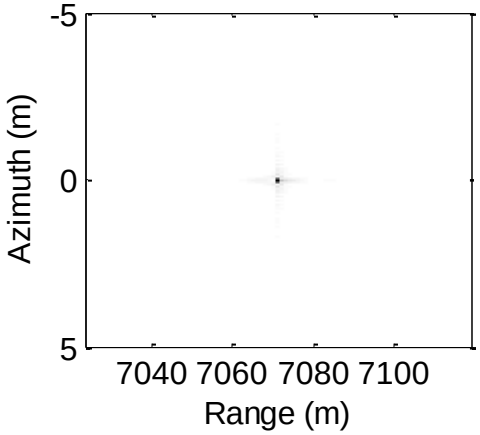
-5
0
5
Azimuth (m)
7040 7060 7080 7100
Range (m)
(b)

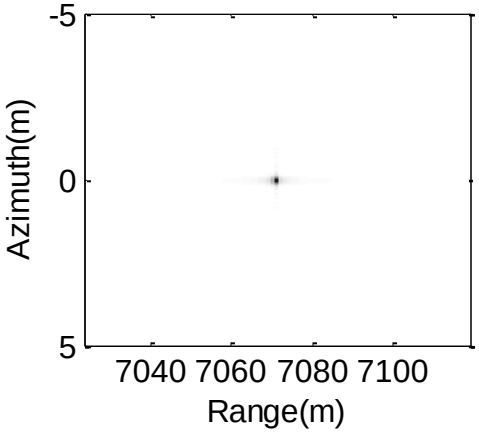
-5
0
5
Azimuth(m)
7040 7060 7080 7100
Range(m)
(c)

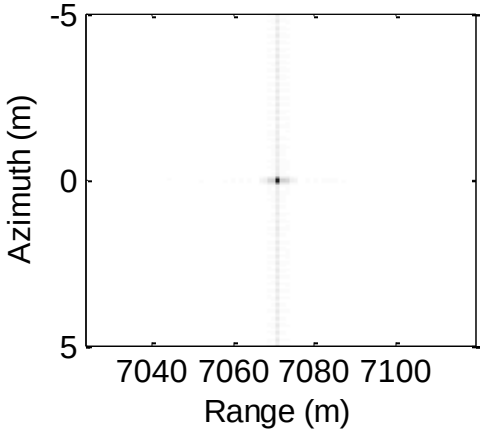
-5
0
5
Azimuth (m)
7040 7060 7080 7100
Range (m)
(d)

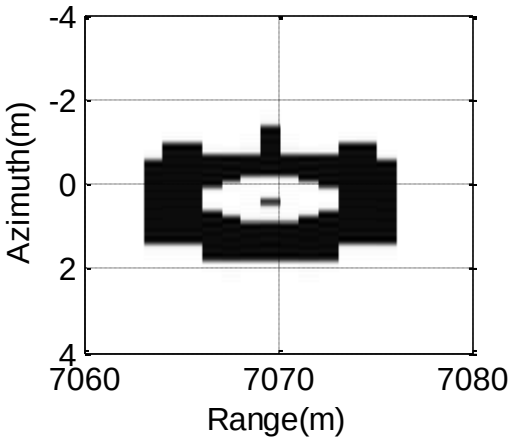
-4
-2
0
2
4
Azimuth(m)
7060
7070
7080
Range(m)
(e)

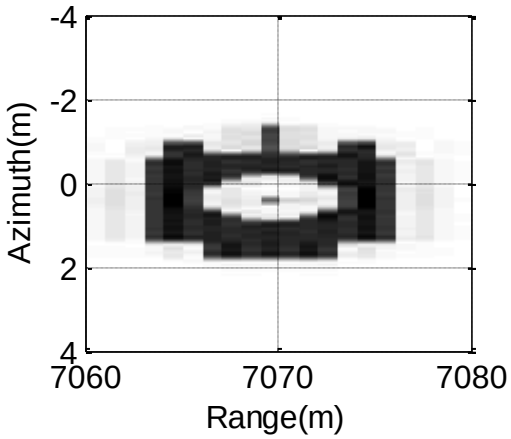
-4
-2
0
2
4
Azimuth(m)
7060
7070
7080
Range(m)
(f)

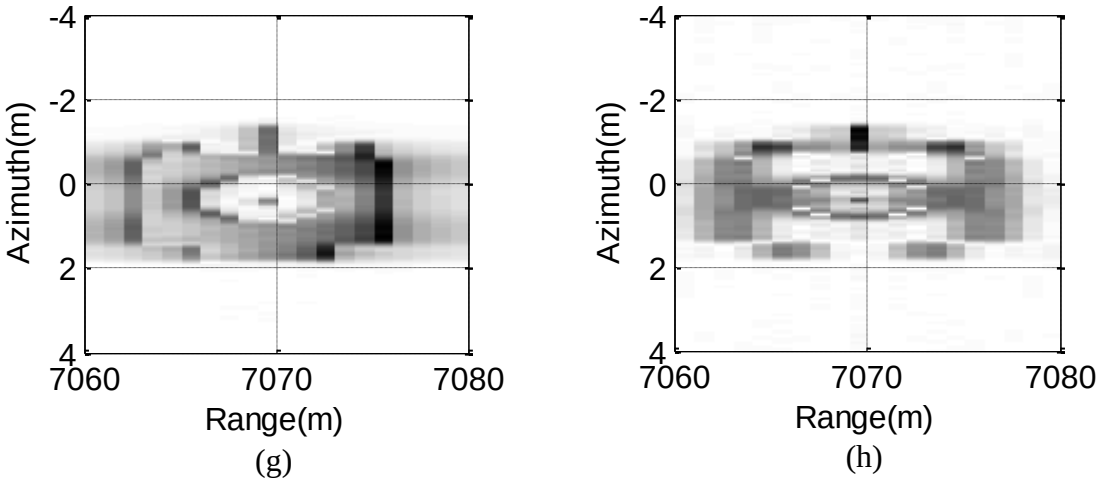

Figure 3.7 Imaging results of synthetic aperture radar for a single point target and tank target. (a) CP-based OFDM single point target. (b) LFM single point target. (c) Conventional OFDM single point target. (d) Random noise single point target. (e) CP-based OFDM tank. (f) LFM tank. (g) Conventional OFDM tank. (h) Random noise tank

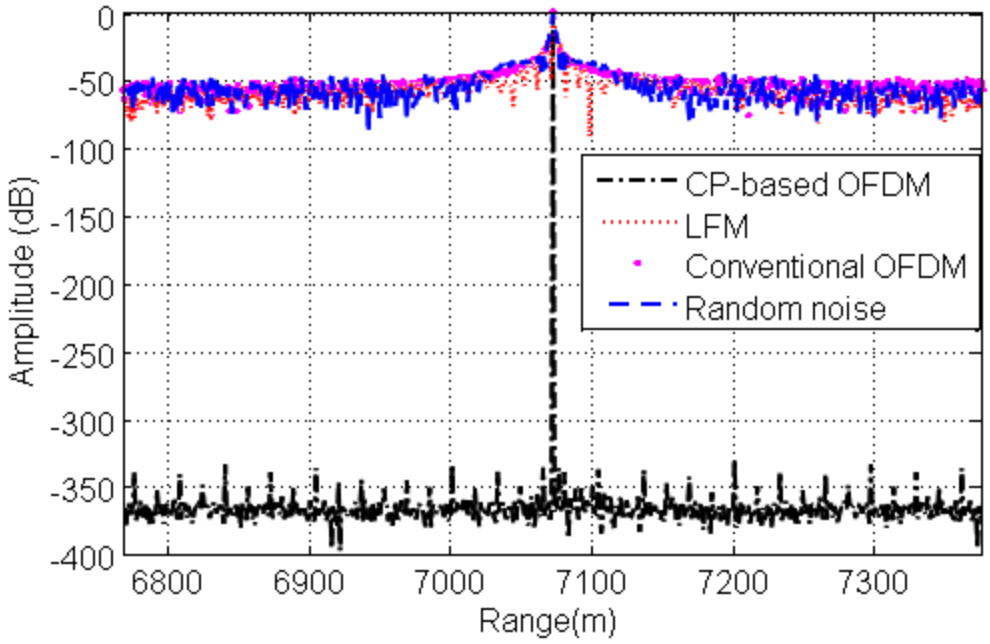

Figure 3.8 Range profiles of the spread function

3.4 Chapter Summary

In this chapter, OFDM with CP for SAR has been investigated and simulated. The RPR of CP-based OFDM signal has been elaborated with the algorithm for the reconstruction of the azimuth profile. Finally, a simulation has been carried out with two different types of targets, single point target and extended target with the shape of the tank, to investigate the performance of this type of signal with already existing signals as conventional OFDM signal, the random noise signal, and LFM signal.

CHAPTER 4

UWB OFDM SYNTHETIC APERTURE RADAR WITH SUFFICIENT CYCLIC PREFIX FOR FOLIAGE PENETRATION (FOPEN)

4.1 Introduction

The purpose of this chapter is to investigate the use of UWB CP-OFDM signal for SAR FOPEN. The model of foliage penetration will be described in Section 4.2, in which the phase and the amplitude characteristics of the foliage are detailed due to its application in this chapter. Furthermore, the algorithm for the reconstruction of the image of targets, which are camouflaged or hidden in forests and tree-lines using SAR will be described. Finally, a summary of the current chapter will be given and motivation of the next chapter will be briefly mentioned.

4.2 Foliage Penetration Model

The model, that is going to be adapted for the modeling of foliage characteristic in this section, is a statistical physical model which was developed at the University of Nebraska-Lincoln (UNL). The FOPEN radar imaging will be introduced in the frequency domain as illustrated in Figure 4.1. $F_T(\omega,\eta)$ and $F_R(\omega,\eta)$ are the foliage propagation characteristics for the transmitted waveform and the target scattered waveform

respectively while $G_F(\omega,\eta)$ represents the total received obscured signal. The range profile of the foliage obscured target in the frequency domain can be expressed as the following:

$$\begin{aligned} G_F(\omega,\eta) &= S(\omega)F_T(\omega,\eta)G(\omega,\eta)F_R(\omega,\eta) \\ &= G_s(\omega,\eta)F(\omega,\eta) \end{aligned} \tag{4.1}$$

where $F(\omega,\eta) = F_T(\omega,\eta)F_R(\omega,\eta)$ represents the frequency and the flight path dependent for the two-way foliage transmission at specified grazing angle and polarization.

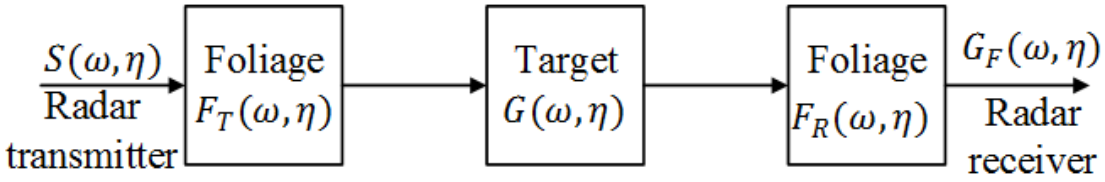

Figure 4.1 Foliage penetration SAR

The model of the two-way foliage transmission according to [20] can be represented by a transfer function which has nonlinear amplitude characteristic and nonlinear phase characteristic. This transfer function at specific polarization can be written as

$$F(\omega,\eta,\gamma_g) = A(\omega,\eta,\gamma_g)exp[j\boldsymbol{\Phi}(\omega,\eta,\gamma_g)] \tag{4.2}$$

where $A(\omega,\eta,\gamma_g)$ indicates the nonlinear amplitude characteristic and $\Phi(\omega,\mu,\gamma_g)$ indicates the nonlinear phase characteristic. Both the amplitude A and the phase Φ are being functions of the radar frequency, the azimuth path, and the grazing angle γ_g.

4.1.1 Amplitude Characteristics

The amplitude characteristics consist of two parts, the attenuation's mean and the fluctuation of the amplitude which can be represented as.

$$A(\omega, \eta, \gamma_g) = A_0(\omega, \gamma_g)[1 + \delta_A(\omega, \eta, \gamma_g)] \tag{4.3}$$

where the mean attenuation is represented by $A_0(\omega, \gamma_g)$and the normalized amplitude fluctuation is $\delta_A(\omega, \eta, \gamma_g)$.

Mean Attenuation

According to [20], the attenuation due to the foliage can be written as the following:

$$A_0(\omega, \gamma_g) = \beta f^{\alpha} \sin(45/\sin(\gamma_g)) \tag{4.5}$$

where $A_0(\omega, \gamma_g)$ is in dB, f is the radar frequency in MHz, $\gamma_g$is the grazing angle to the local clutter patch. The representative values of α and β were determined as in [20] and summarized in Table 4.1.

Table 4-1 Foliage attenuation model parameters

Mean attenuation Model		
Polarization	α	β
HH	0.79	0.05
VV	0.5	0.45

Amplitude Fluctuation

The normalized amplitude fluctuation $\delta_A(\omega, u, \gamma_g)$ consists of two components, the frequency and grazing angle dependent $\delta_\omega(\omega, \gamma_g)$ and the fluctuation of the amplitude along the flight path which can be written as the following:

$$\delta_A(\omega, \eta, \gamma_g) = \delta_\omega(\omega, \gamma_g)\delta_\eta(\eta) \tag{4.6}$$

The frequency and the grazing angle dependent are modeled as random process where the random variable has

$$x = A_0(\omega, \gamma_g)[1 + \delta_\omega(\omega, \gamma_g)] \tag{4.7}$$

Log-Gamma probability density, i.e., when the random variable x is expressed in *dB*, it has a Gamma density, represented as

$$p(x, a, b) = \frac{1}{b^a \Gamma(a)} x^{a-1} e^{-x/b} \tag{4.8}$$

where a and b are two constants to be specified. The mean and the variance of the Gamma distribution are $\mu = ab$ and $\sigma^2 = ab^2$, respectively.

The fluctuation of the amplitude along the flight path $\delta_\eta(\eta)$ is modeled as

$$\delta_\eta(\eta) = \exp(\eta_H(\Delta\eta)) \tag{4.9}$$

where $\eta_H(\Delta\eta))$ represents the fractional Brownian motion (fBm) random process which has two parameters, the Hurst exponent $H \simeq 0.4$ for cover vegetation [20] and $\Delta\eta$ which depend on the size of the synthesized aperture.

4.1.2 Phase Characteristics

The phase characteristics also have two parts, the linear phase and the fluctuation of the phase which can be represented as in [20].

$$\Phi(\omega,\eta,\gamma_g) = -P_0\omega + \delta_\phi(\omega,\eta,\gamma_g) \tag{4.10}$$

where the linear phase is $P_0\omega$ and the phase fluctuation is represented by $\delta_\phi(\omega,\eta,\gamma_g)$. Based on [16], the fluctuation of the phase can be obtained from the fluctuation of the amplitude with the assumption that the incoherent field's phase is uniformly distributed between $-\pi$ and π, which can be written as the following:

$$\delta_\phi(\omega,\eta,\gamma_g) = \tan^{-1}\left[\frac{\delta_A(\omega,\eta,\gamma_g)sin(\psi)}{1+\delta_A(\omega,\eta,\gamma_g)\cos(\psi)}\right] \tag{4.11}$$

where ψ has a uniform density over $[-\pi,\pi]$.

The received raw radar data along the range direction will be transformed into the frequency domain in order to incorporate the effect of the foliage obscured into the reconstructed image as illustrated in Figure.4.2 and mathematically can be written as

$$G_k(\omega,\eta) = Z_k * F_k(\omega,\eta,\gamma_g) + w_k, k = 0,1,\dots,N+2M-3 \tag{4.12}$$

where $Z_k = \frac{1}{\sqrt{N}}\sum_{n=0}^{N+2M-3} z_n exp\left\{\frac{-j2\pi kn}{N}\right\}$ which is the FFT on the received vector z and $*$ indicates multiplication. After that IFFT is applied along the range direction to get the time-domain version of received echo and the processing for the reconstruction of SAR FOPEN is illustrated in Figure 4.2.

4.3 Simulation and Performance Discussion

MATLAB simulation has been carried out to investigate the UWB CP-based OFDM SAR and UWB random noise SAR for the application of FOPEN using the following parameters as in Table 4.2. The population of the symbols in the frequency domain over the UWB CP-based OFDM SAR's subcarriers is considered to be vectors of the binary pseudorandom noise sequence corresponding to values of -1 and 1. The random noise signal is a band-limited wide-sense stationary (WSS) Gaussian process with zero mean and variance σ^2 which can be written as in [40]

$$s(t) = s_I(t)\cos(2\pi f_0 t) - s_Q(t)\sin(2\pi f_0 t) \tag{4.13}$$

where $s_I(t)$ and $s_Q(t)$ are Gaussian random processes, and f_0 is the central frequency and the reconstruction of SAR image is shown in Figure 4.3.

Two scenarios have been considered for the target to be imaged. First, a single point target is located at the center of the swath width. The images of single point target with HH polarization of CP-based OFDM and random noise are illustrated in Figure 4.2(a) and Figure 4.2 (b) and alike for the VV polarization is illustrated in Figure 4.2 (c) and Figure 4.2 (d) respectively. It is clear that the CP-based OFDM SAR has superior performance compared to random noise SAR.

Most importantly, it is clear that the image of SAR for FOPEN in Figure 4.2(e), Figure 4.2 (f), Figure 4.2 (g) and Figure 4.2 (h) are distorted due to the foliage effect which leads to the fluctuation of the side lobes.

The normalized range profiles of the UWB CP-based OFDM signal and UWB random noise signals without application to FOPEN and with application to FOPEN are illustrated in Figure 4.5 and Figure 4.6 respectively. It can be noticed that the side lobes for UWB CP-based OFDM signal are lower than of the UWB random noise's side lobes.

The normalized azimuth profiles of the point spread function of the two signals are illustrated in Figure 4.7 and Figure 4.8. It can be seen that the azimuth profiles either for the application to FOPEN or without the application to FOPEN are similar for both of the two signals.

Moreover, for better clarification, two measures has been used to investigate the performance of UWB CP-based OFDM SAR for FOPEN compared to the random noise SAR for the FOPEN which are the integrated side lobe level ratio (ISLR) and the peak side lobe level ratio (PSLR)

ISLR is defined as the ratio of the total several side lobes on both sides of the main lobe to the main lobe which is expressed in decibels as the following:

$$ISLR = 10\log\left(\frac{power\ integrated\ over\ sidelobes}{total\ main\ lobe\ power}\right) \quad (4.14)$$

PSLR is defined as the ratio between the height of the largest side lobe and the height of the main lobe which is expressed in decibels as the following:

$$PSLR = 10\log\left(\frac{power\ integrated\ over\ sidelobes}{total\ main\ lobe\ power}\right) \quad (4.15)$$

The results of these metrics for the two signals are illustrated in tables 4.3 and 4.4. The results in table 4.3 are related to Figures 4.5 and 4.7 and the results in table 4.4 are related

to Figures 4.6 and 4.8. It can be clear that the UWB CP-based OFDM signal has lower ISLR and PSLR compared to the UWB random noise signal along the range direction, while in the azimuth direction are the same. Similarly, for the application of FOPEN, the UWB CP-based OFDM signal has lower ISLR and PSLR than the UWB random noise signal along the range direction, while in the azimuth direction they are the same.

Table 4-2 List of simulation parameters of CP-based OFDM SAR for foliage penetration

Parameters (units)	Symbols	Units	Value
Pulse repetition frequency	PRF	Hz	800
Bandwidth	B	GHz	4
The sampling frequency	f_s	GHz	4
the antenna length	L_a	m	1
the carrier frequency	f_c	GHz	9
The synthetic Aperture time	T_a	sec	1
The effective speed of the moving radar	v_p	m/s	150
The platform height of the antenna	H_p	km	5
The slant range swath center	R_c	km	$5\sqrt{2}$
The number of range cells	M	-	96
The duration of OFDM signal without CP	T	us	0.256
The number of OFDM subcarriers	N	-	1024
The length of the CP	CP_{length}	-	95
The duration of CP	T_{GI}	us	0.02375
The duration of CP-based OFDM pulse	T_0	us	0.27975

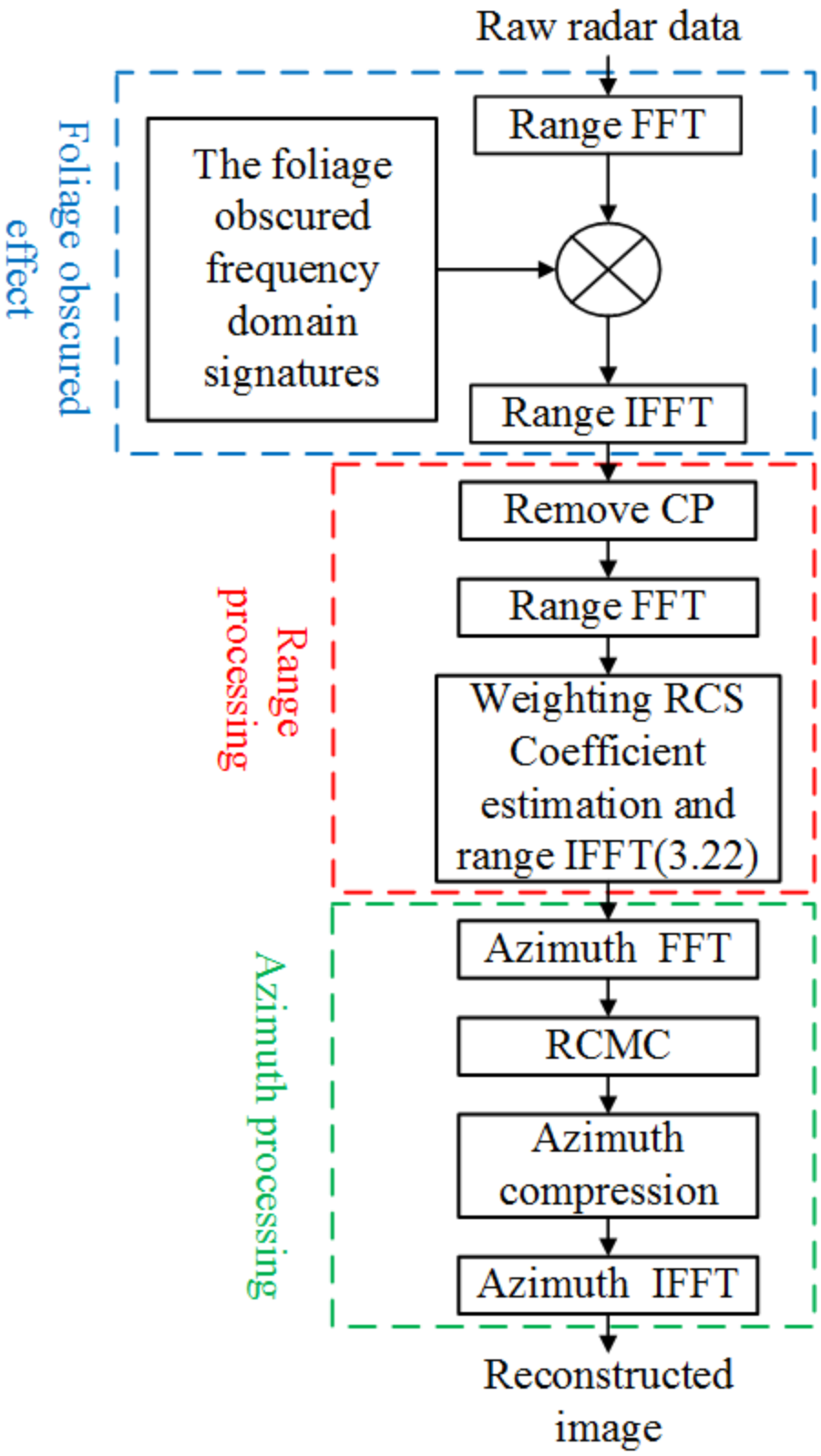

Figure 4.2 Block diagram of UWB CP-based OFDM SAR for FOPEN

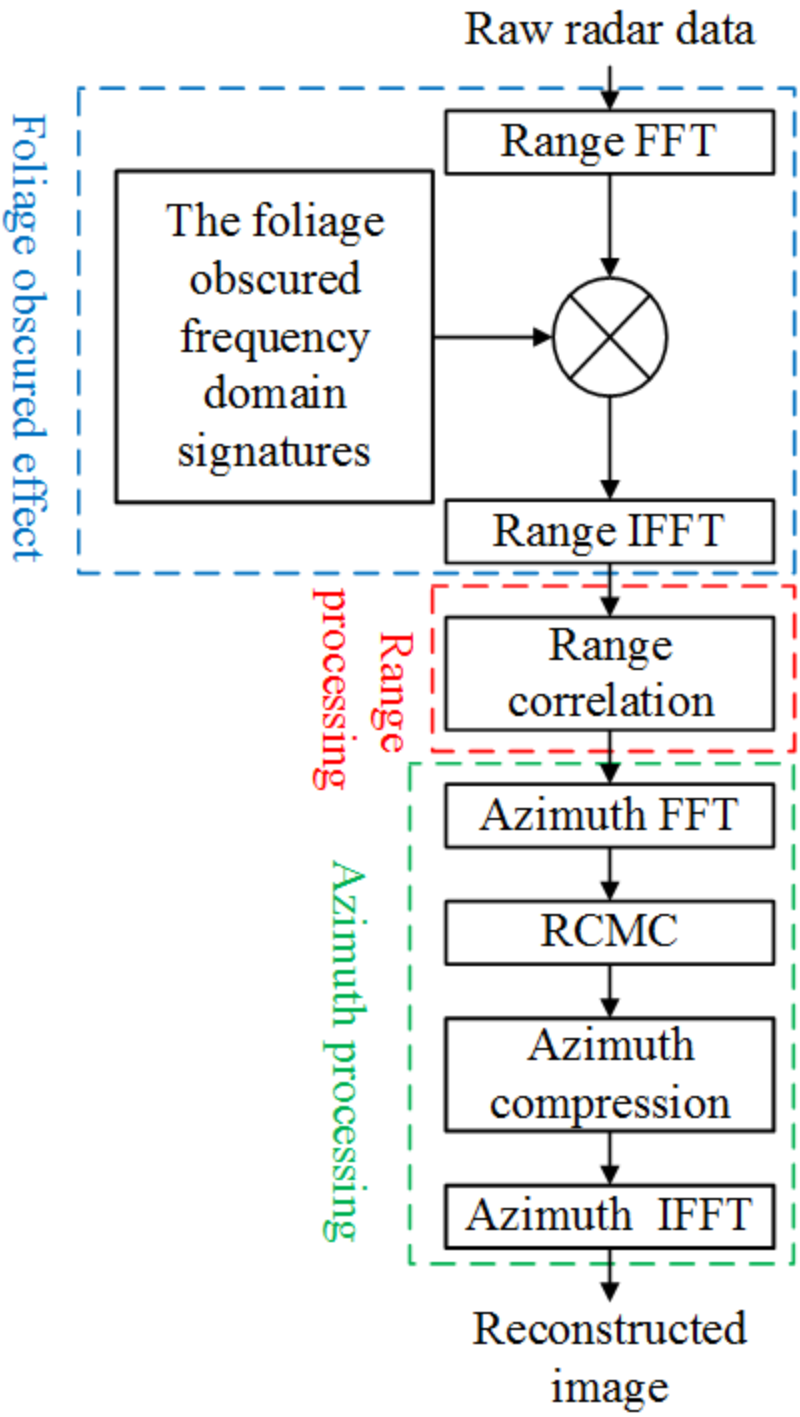

Figure 4.3 Block diagram of UWB random noise SAR for FOPEN

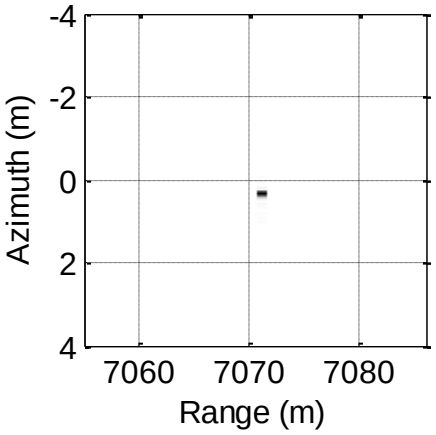
-4
-2
0
2
4
Azimuth (m)
7060
7070
7080
Range (m)

(a)

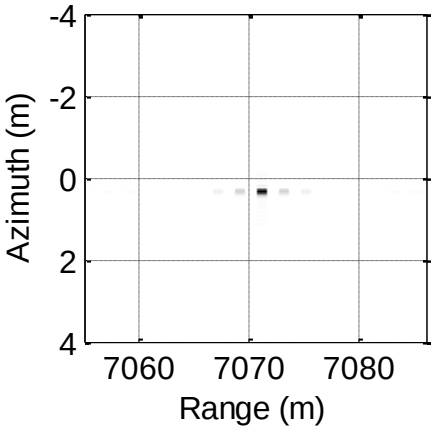
-4
-2
0
2
4
Azimuth (m)
7060
7070
7080
Range (m)

(b)

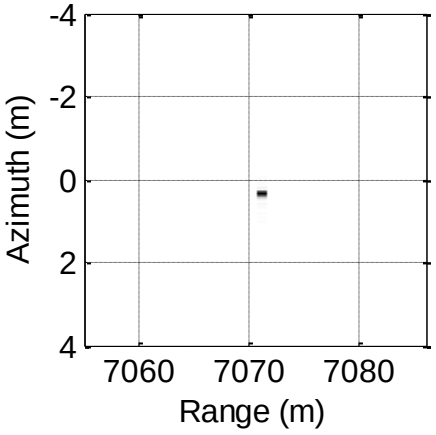
-4
-2
0
2
4
Azimuth (m)
7060
7070
7080
Range (m)

(c)

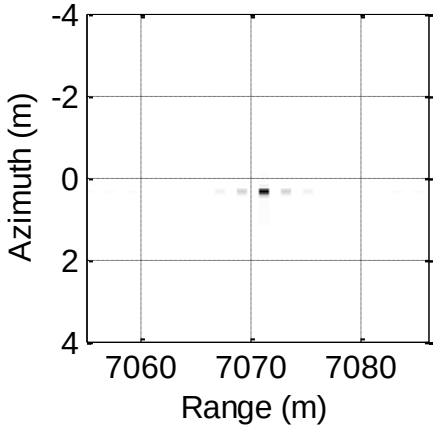
-4
-2
0
2
4
Azimuth (m)
7060
7070
7080
Range (m)

(d)

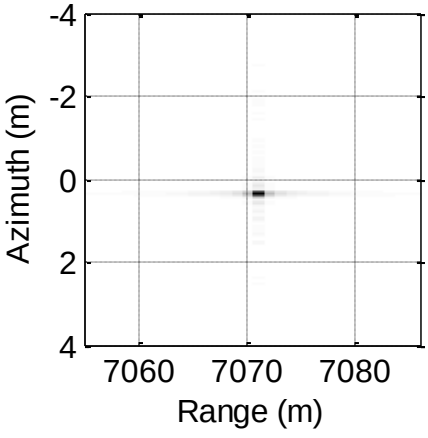
-4
-2
0
2
4
Azimuth (m)
7060
7070
7080
Range (m)

(e)

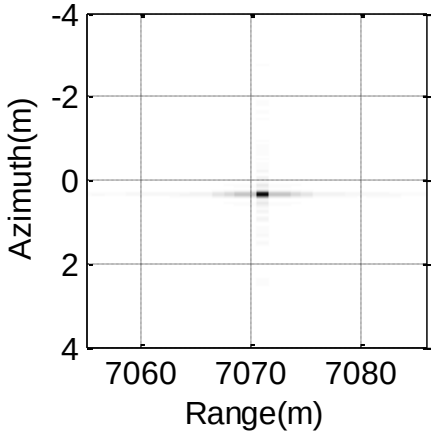
-4
-2
0
2
4
Azimuth(m)
7060
7070
7080
Range(m)

(f)

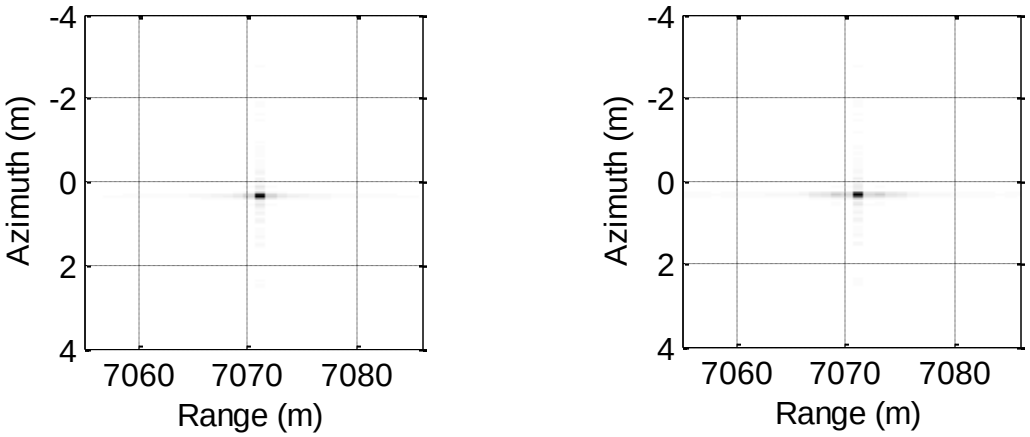

(g) (h)

Figure 4.4 Imaging results of UWB synthetic aperture radar for a single point target. (a) CP-based OFDM SAR HH. (b) Random noise SAR HH. (c) CP-based OFDM SAR VV. (d) Random noise SAR VV. (e) CP-based OFDM SAR FOPEN HH. (f) Random noise SAR FOPEN HH. (g) CP-based OFDM SAR FOPEN VV. (h) Random noise SAR FOPEN VV.

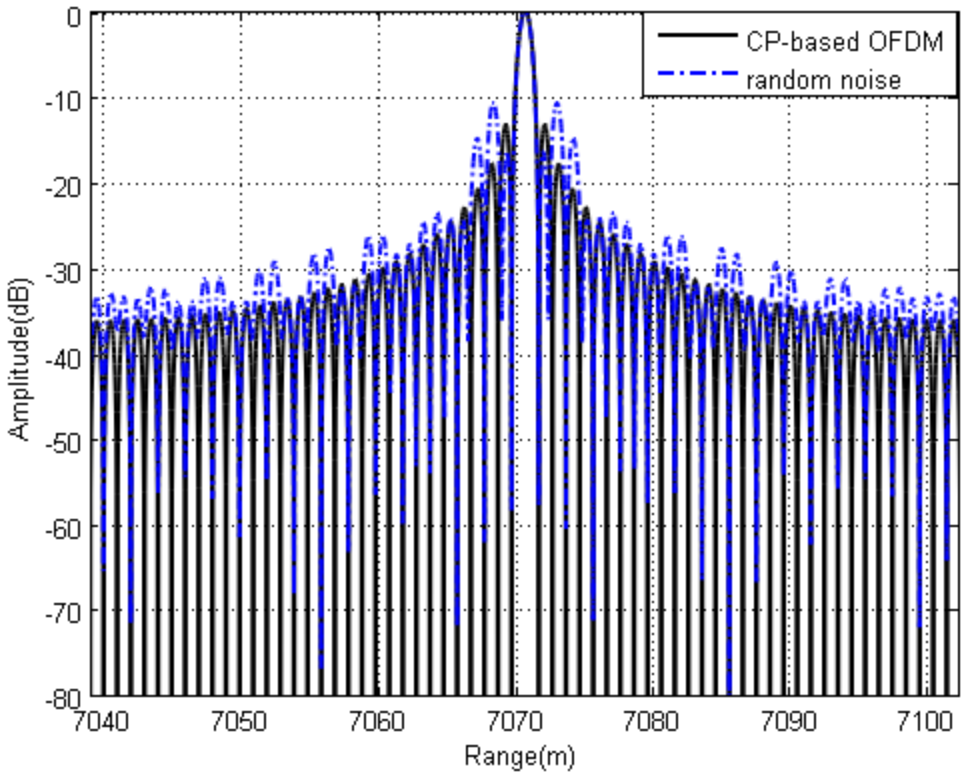

Figure 4.5 Range profiles of the spread function

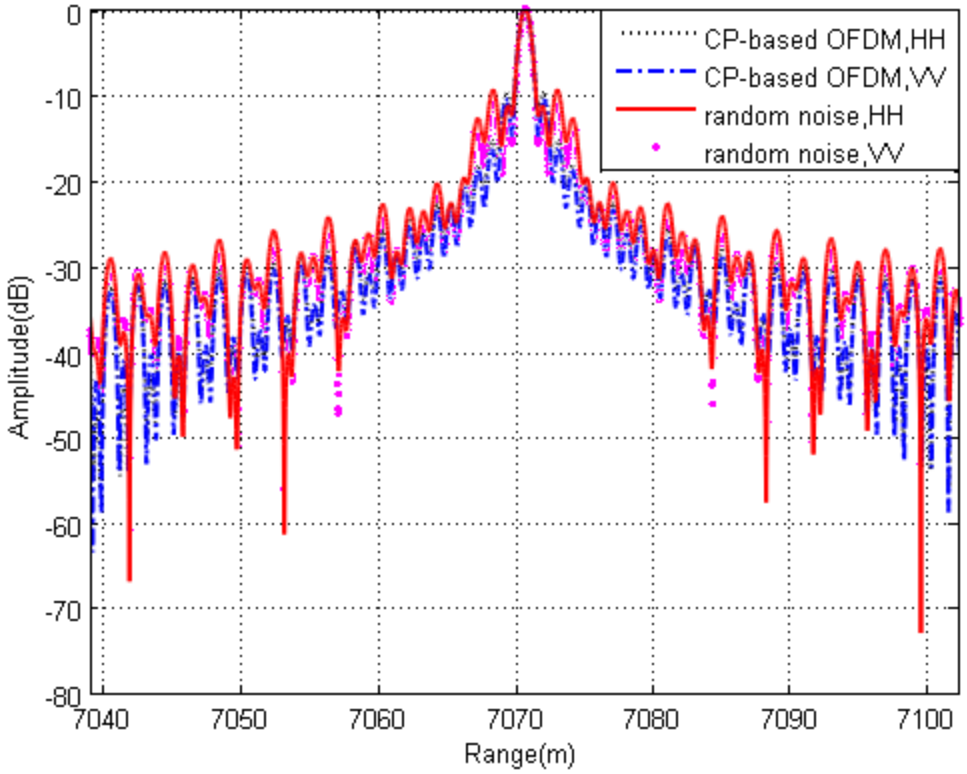

Figure 4.6 Range profiles of the spread function with application to FOPEN

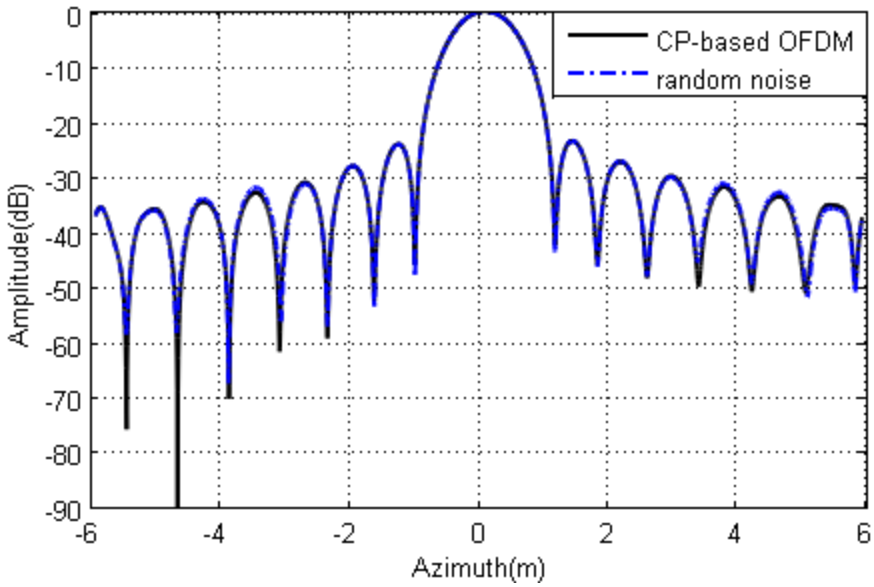

Figure 4.7 Azimuth profiles of the spread function

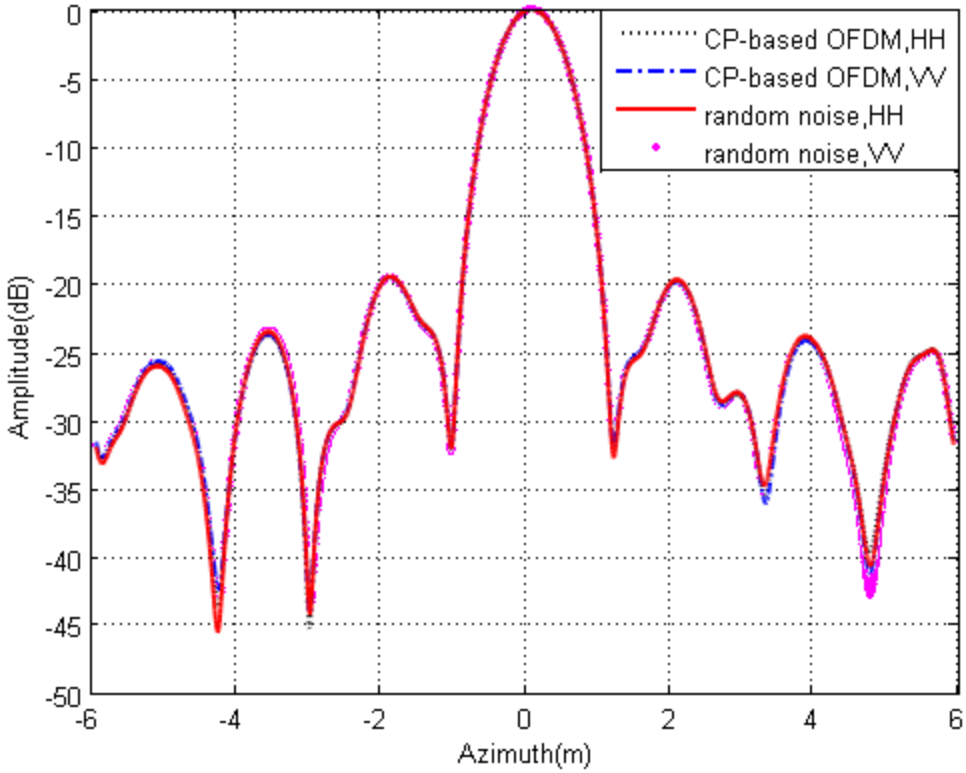

Figure 4.8 Azimuth profiles of the spread function with application to FOPEN

Table 4-3 Results of image quality metrics for UWB CP-OFDM and UWB random noise SAR

Method	CP-OFDM, HH	Random noise, HH	CP-OFDM, VV	Random noise, VV
$ISLR_{dB}$				
Range	-9.68	-6.47	-9.68	-6.47
Azimuth	-21.78	-21.71	-21.78	-21.71
$PSLR_{dB}$				
Range	-13.26	-10.71	-13.26	-10.71
Azimuth	-23.49	-23.49	-23.49	-23.49

Table 4-4 Results of image quality metrics for UWB CP-OFDM and random noise SAR for FOPEN

Method	CP-OFDM FOPEN, HH	Random noise FOPEN, HH	CP-OFDM FOPEN, VV	Random noise FOPEN, VV
$ISLR_{dB}$				
Range	-5.63	-3.37	-6.49	-4.18
Azimuth	-15.26	-15.24	-15.29	-15.25
$PSLR_{dB}$				
Range	-9.76	-9.49	-10.57	-10.06
Azimuth	-19.52	-19.52	-19.54	-19.52

We then further extend the work by considering an extended target with the shape of a tank by the arrangement of few single point targets. The results are illustrated in Figure 4.9. It can be clearly noticed that the UWB CP-based OFDM signal for both of the two scenarios, SAR and SAR FOPEN, is better than the UWB random noise signal.

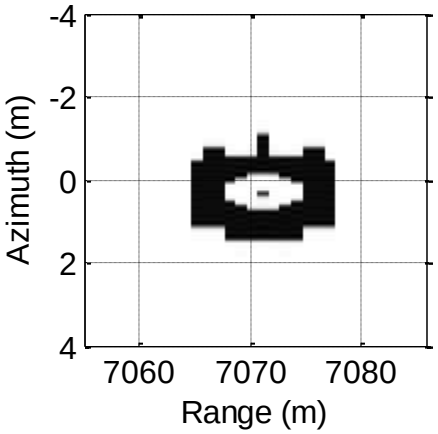
-4
-2
0
2
4
Azimuth (m)
7060
7070
7080
Range (m)

(a)

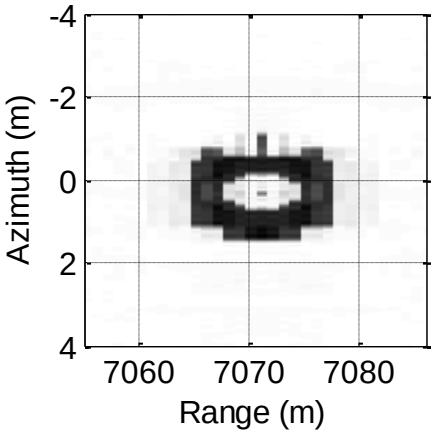
-4
-2
0
2
4
Azimuth (m)
7060
7070
7080
Range (m)

(b)

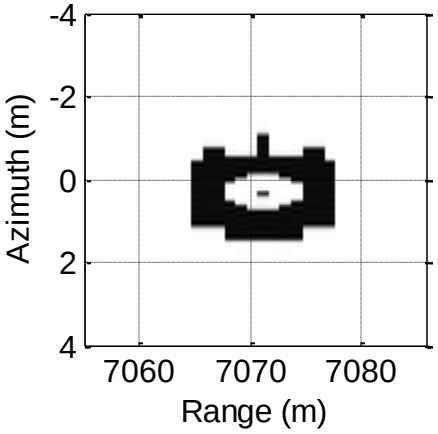
-4
-2
0
2
4
Azimuth (m)
7060
7070
7080
Range (m)

(c)

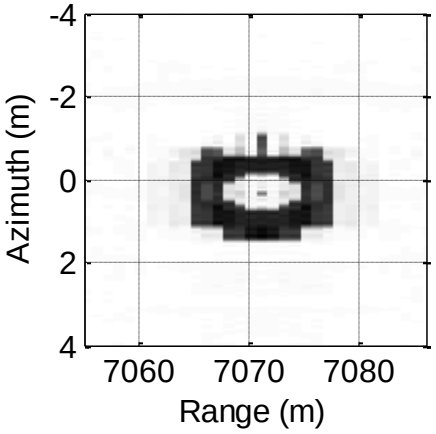
-4
-2
0
2
4
Azimuth (m)
7060
7070
7080
Range (m)

(d)

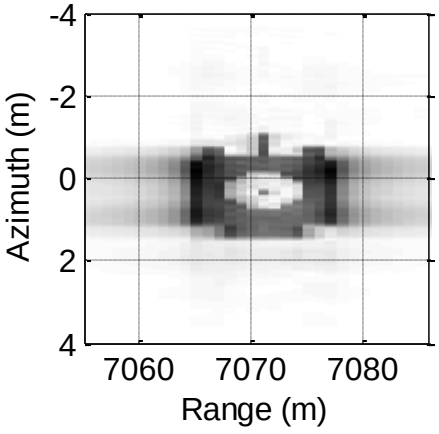
-4
-2
0
2
4
Azimuth (m)
7060
7070
7080
Range (m)

(e)

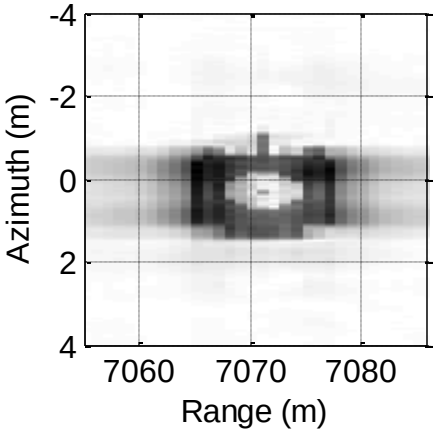
-4
-2
0
2
4
Azimuth (m)
7060
7070
7080
Range (m)

(f)

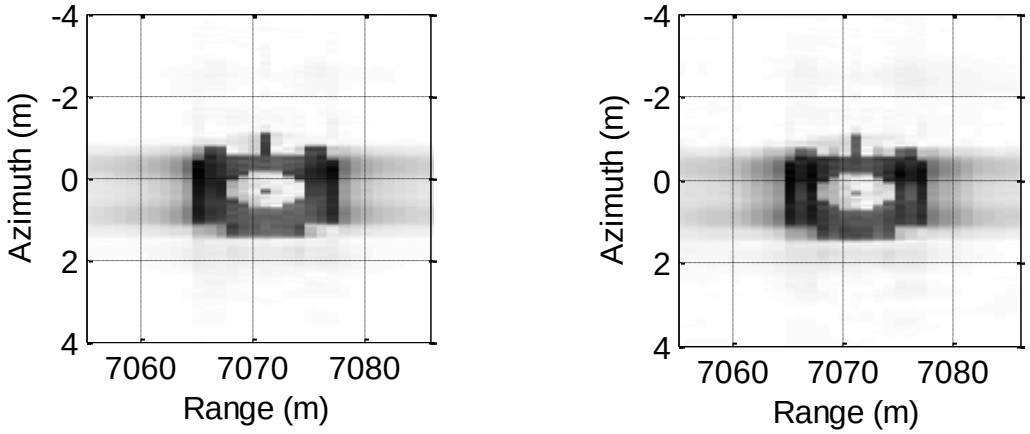

(g) (h)

Figure 4.9 Imaging results of UWB synthetic aperture radar for the extended target. (a) CP-based OFDM SAR HH. (b) Random noise SAR HH. (c) CP-based OFDM SAR VV. (d) Random noise SAR HH. (e) CP-based OFDM SAR FOPEN HH. (f) Random noise SAR FOPEN HH. (g) CP-based OFDM SAR FOPEN VV. (h) Random noise SAR FOPEN VV

4.4 Chapter Summary

This chapter focused on the use of the latest development of OFDM signal in SAR for the application for FOPEN. First of all, the model that was used in this study to model the effect of the foliage has been elaborated. Then this model has been combined with the algorithm to process the raw data of SAR using the CP-based OFDM signal to get the final image of two targets, single point target and extended. Furthermore, the performance of CP-based OFDM SAR for FOPEN application has been compared with the UWB random noise signal and found that the first has lower ISLR and PSLR compared to the later along the range direction.

CHAPTER 5

FRACTIONAL FOURIER TRANSFORM-BASED OFDM SYNTHETIC APERTURE RADAR

5.1 Introduction

This chapter proposes OFDM signal based on the FrFT instead of the DFT for SAR application. It is the first investigation for the use of FrFT in the construction of OFDM signal at the transmitter side for SAR application. First of all, the concept of FrFT with the computation is introduced briefly. Secondly, the method for the reconstruction of the range profile for SAR based on the FrFT-based OFDM signal is developed. Moreover, the performance of FrFT-based OFDM SAR image has been illustrated by considering two types of targets, single point target and arrangement of a few single point targets in a way represented as an extended target shape (i.e., tank). Finally, a short summary is given for recapitulating the current chapter.

5.2 Fractional Fourier Transform-based OFDM Range Profile Reconstruction

The FrFT is the generalization method of the Fourier transform. The FrFT of defined signal as $x(t)$ is denoted as $F_{\alpha}(u)$ where $\alpha = p\pi/2$ is the angle of FrFT and p is the FrFT order.

$$F_\alpha(u)\{F^p[x(t)]\}(u) = \int_{-\infty}^{\infty} x(t)K_\alpha(t,u)\,dt \tag{5.1}$$

And its inverse FrFT (IFrFT) is represented as the following:

$$x(t) = \int_{-\infty}^{\infty} F_\alpha(u)K_{-\alpha}(t,u)dt \tag{5.2}$$

where $K_\alpha(t,u)$ is the transform kernel of the FrFT which is represented as the following:

$$K_a(t,u) = \begin{cases} \sqrt{\dfrac{1-jcot\alpha}{2\pi}}\,exp\left(j\dfrac{t^2+u^2}{2}cot\alpha - jutcsc\alpha\right), & \alpha \neq n\pi \\ \delta(t-u), & \alpha = 2n\pi \\ \delta(t+u), & \alpha = (2n\pm 1)\pi \end{cases} \tag{5.3}$$

The u domain is known as the fractional Fourier domain, while time and frequency domain can be represented as special case when $p = 1$.

Without loss of generality, we consider that the angle of the FrFT is satisfied with $0 < \alpha < 2\pi$, which corresponds to $0 < p < 2$. Therefore, the discrete fractional Fourier transform (DFrFT) as in [25] can be written as

$$s(t) = e^{\left(-\frac{j}{2\cot(\alpha)t^2}\right)} \sum_{k=0}^{N-1} e^{\left(-j/2\cot(\alpha)k^2\Delta u^2\right)} e^{(jtk\Delta u/sin\alpha)} x(k) \qquad t = 0 \sim (N-1)\Delta t, \tag{5.4}$$

where the fractional domain and the time domain sampling interval are represented by Δu and Δt respectively. The discrete sampling of the input signal is $x(k)$ with total points equal to N. The number of sampling points in the fractional domain and in the time domain is both equal to N. For the sake of preserving the mutual orthogonality between

the FrFT-based OFDM subcarriers, the sampling period in the fractional domain must be as in [25].

$$\Delta u = \frac{2\pi \sin \alpha}{N\Delta t} \tag{5.5}$$

5.3 FrFT-OFDM SAR Signal Model

Giving the geometry of monostatic stripmap SAR in Figure 3.1, the radar is carried on airplane moving parallel to the azimuth direction with instantaneous coordinate $\left(0, y_p(\eta), H_p\right)$ .The time at which the radar transmit signal along the flight path is η and H_p is the radar platform's height. T_a is defined as the time extent along the flight over which the target on the ground lies in the antenna beam, synthetic aperture time. Assume that at the transmitter side, FrFT-OFDM signal with Bandwidth equal to B Hz distributed between N subcarriers separated by $\Delta f = \frac{B}{N} = 1/T$ and let $\boldsymbol{S} = [S_0, S_1, \dots, S_{N-1}]$ be the population of the symbols in the frequency domain over the subcarriers. Then discrete fractional domain-OFDM signal is the IFrFT of the vector $\boldsymbol{S}$ and the FrFT-OFDM pulse is represented as the following:

$$s(t) = e^{\left(-\frac{j}{2cot(\alpha)t^2}\right)} \sum_{k=0}^{N-1} e^{\left(-j/2cot(\alpha)k^2\Delta u^2\right)} e^{(jtk\Delta u/sin\alpha)} S(k) \qquad t = 0 \sim (N-1)\Delta t, \tag{5.6}$$

Once the signal received and demodulated to baseband at the receiver side, the complex envelope of the received signal from fixed point target lies in the m^{th} cell along the range direction can be represented in terms of the fast time η and the slow time t as the following:

$$u_m(t,\eta) = g_m \varepsilon_a(\eta)\, exp\left\{-j4\pi f_c \frac{R_m(\eta)}{c}\right\} s\left(t - \frac{2R_m(\eta)}{c}\right) + w(t,\eta),$$
$$t\epsilon\left[\frac{2R_m}{c}, \frac{2R_m(\eta)}{c} + T\right] \quad (5.7)$$

where $\varepsilon_a(\eta) = p_a^2(\theta(\eta))$ is the azimuth beam that governs the strength of the received signal along the azimuth direction, $p_a(\theta) \approx sinc\,(0.886\,\theta/\beta_{bw})$, θ is the boresight's angle measured in plane of the slant range, $\beta_{bw} = 0.886\lambda\,/L_a$ is beamwidth along the azimuth, L_a is the antenna's length, g_m is the RCS coefficient that arise from the targets that lie in the m^{th} cell along the range direction located inside the beam of the radar on the ground, c is the speed of the light, $\omega(t,\eta)$ represent the noise, and the distance, the slant range, between the radar and the target in the m^{th} cell along the range direction located at $(x_m, y_m, 0)$ can be represented as the following:

$$R_m(\eta) = \sqrt{\bar{R}_m^2 + \left(y_m - y_p(\eta)\right)^2} = \sqrt{\bar{R}_m^2 + v_p^2\eta^2} \quad (5.8)$$

where v_p is the platform's velocity on which the radar is carried and $\bar{R}_m = \sqrt{x_m^2 + H_P^2}$ is the closest approach between the radar and the target in the m^{th} cell along the range direction.

The received signal from every range cell within the swath width can be represented as the following:

$$u(t,\eta) = \sum_m u_m(t,\eta). \quad (5.9)$$

After that, the received signal at the receiver side is sampled with $T_s = \frac{1}{B}$ as the sampling interval and the resolution along the range direction is $\rho_r = \frac{c}{2B}$. Presume that the swath

width for the radar is R_w. The swath width of the radar can be partitioned into M cells along the range direction as shown in Figure 5.2. The response of each range cell is constructed by the summation of the responses of all scatterers in this range cell with their own delay and phase and the number of M Range cells can be written as

$$M = \frac{R_w}{\rho_r} \tag{5.10}$$

From Figure 5.2, we notice that $R_m(\eta) = R_0(\eta) + m\rho_r$. Therefore, $\left(t - \frac{2R_m(\eta)}{c}\right)$ in (5.7) can be represented as the following:

$$t - \frac{2R_m(\eta)}{c} = t - \frac{2(R_0(\eta) + m\rho_r)}{c} = t - t_0(\eta) - mT_s \tag{5.11}$$

where $t_0(\eta) = \frac{2R_0(\eta)}{c}$, the constant time delay for each azimuth time η because it is independent of m.

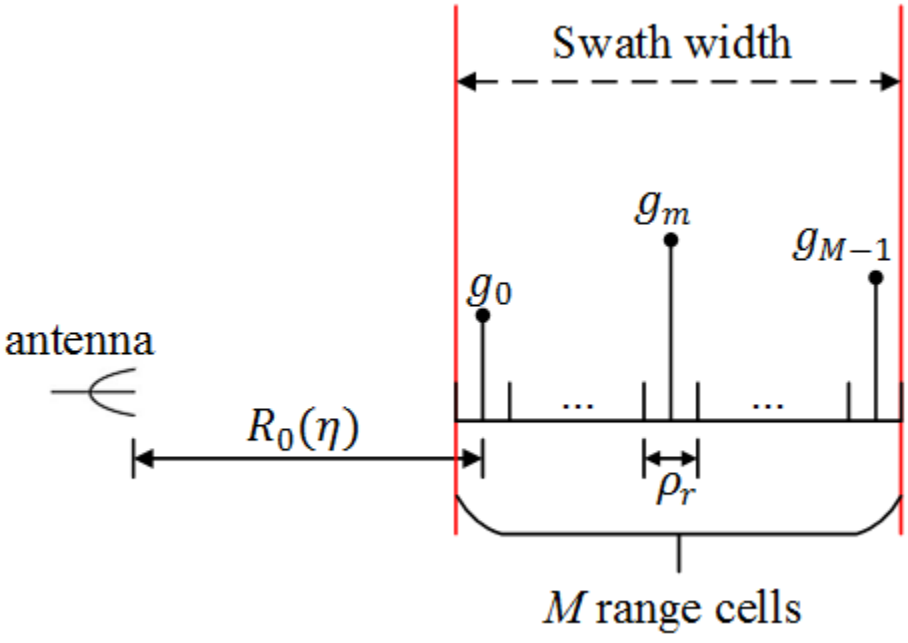

Figure 5.1 Graphical representation of one line along the range direction

Suppose that the sampling was done after $t_0(\eta)$ from the first arrival version of the emitted signal from the transmitter. Therefore, combining with (5.7), (5.11), and (5.9), $u\,(t,\eta)$ can be represented as the discrete time linear convolution of the weighted RCS coefficient d_m with the transmitted sequence as the following:

$$u_i = \sum_{m=0}^{M-1} d_m s_{i-m} + w_i, \qquad i = 0,1,\dots,N-2+M \tag{5.12}$$

where

$$d_m = g_m \varepsilon_a(\eta) exp\left\{-j4\pi f_c \frac{R_m(\eta)}{c}\right\} \tag{5.13}$$

The exponential part $4\pi f_c \frac{R_m(\eta)}{c}$ is the azimuth phase and s_i is the complex envelope of the OFDM Pulse based on the FrFT in (5.4) with time duration $t \in [0,T]$.

Once the signal in (5.12) is received, the final $M-1$ samples are discarded due to the lack of full M RCS coefficients from all the M cells along the range direction, therefore, we obtain

$$u_n = \sum_{m=0}^{M-1} d_m s_{n-m} + w_n, \qquad n = 0,1,\dots,N-1 \tag{5.14}$$

After that, the received signal is correlated with the transmitted sequence to construct the range profile using the DFT. Therefore, we obtain

$$U_k = \frac{1}{\sqrt{N}} \sum_{n=0}^{N+M-2} u_n exp\left\{\frac{-j2\pi kn}{N+M-1}\right\}, k = 0,1,\dots,N-1 \tag{5.15}$$

Then, the range profile can be reconstructed as

$$Z_k = U_k S^*{}_k, \qquad k = 0,1,\dots,N-1 \tag{5.16}$$

where $[S_0, S_1, \dots, S_{N-1}]$ is the FFT of the transmitted sequence vector S in (5.6) and the asterisk denotes complex conjugate.

Then, perform IFFT to obtain the range profile in the time domain as the following:

$$u_m(t,\eta) = \frac{1}{\sqrt{N}} \sum_{k=0}^{N-1} Z_k exp\left\{\frac{j2\pi nk}{N}\right\}, n = 0, \dots, N-1 \tag{5.17}$$

The processing in the azimuth direction is similar to the conventional stripmap SAR imaging [2] as shown in Figure 5.2.

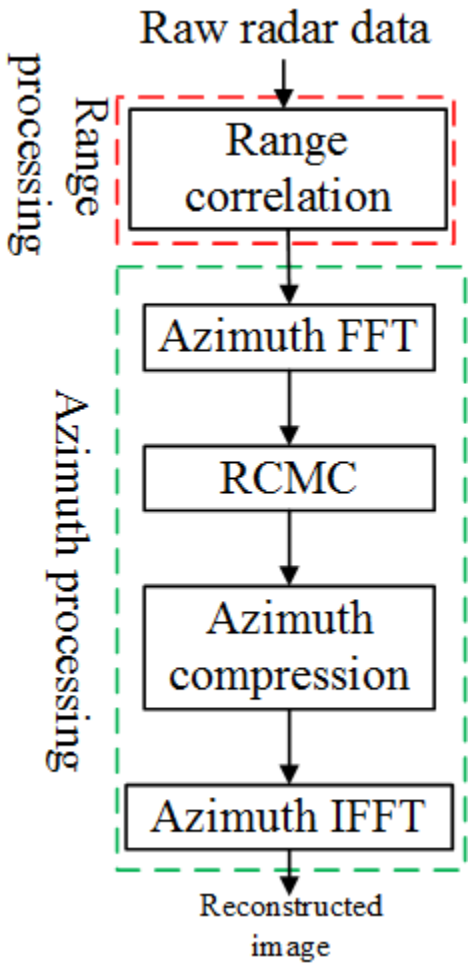

Figure 5.2 Block diagram of FrFT-based OFDM SAR processing

First of all, azimuth FFT is implemented to do the RCMC in the frequency domain followed by the azimuth compression through the matched filter.

5.4 Simulation and Performance Discussion

In this section, we present the results obtained for OFDM SAR based on FrFT with the following parameters in Table 5.1 as a typical SAR system. The population of the symbols over the subcarriers of the FrFT-based OFDM signal is considered to be vectors of PN sequence of values -1 and 1. The angles of fractional Fourier domain which have been adopted are 45 degree , 35 degree, 25 degree, 15 degree and 10 degree.

Two scenarios have been considered for the availability of the target on the ground to be imaged. First, a single point target is located at the center of the swath width. The images of point target are shown in Figure 5.3. It is clear that the FrFT-based OFDM SAR is better than the FFT-based OFDM SAR and FrFT-based OFDM for all the adopted degrees are the same.

Moreover, the normalized range profiles of the point spread function are shown in Figure 5.4, while the normalized azimuth profiles of the point spread function are shown in Figure 5. 5. Furthermore, the quality image metrics such as the ISLR and the PSLR have been investigated in table 5.2 and it indicates that the FrFT-based OFDM SAR is better than the OFDM SAR based on FFT.

Finally, an extended target constructed with the arrangement of a few single point targets to test the performance of OFDM SAR based on the FrFT has been considered and the images of that extended target are shown in Figure 5.6.

Table 5-1 List of simulation parameters of FrFT-based OFDM SAR

Parameters	Symbols	Units	Value
Pulse repetition frequency.	PRF	Hz	800
Bandwidth.	B	MHz	150
Sampling frequency.	f_s	MHz	150
The length of the antenna.	L_a	m	1
The carrier frequency.	f_c	GHz	9
The synthetic aperture time.	T_a	sec	1
The speed of the moving radar.	v_p	m/s	150
The height of platform for the radar.	H_p	km	5
The slant range swath center.	R_c	km	$5\sqrt{2}$
The number of range cells.	M	-	96
The length of the transmitted signal.	T	μs	4.05
The number of the subcarriers.	N	-	607

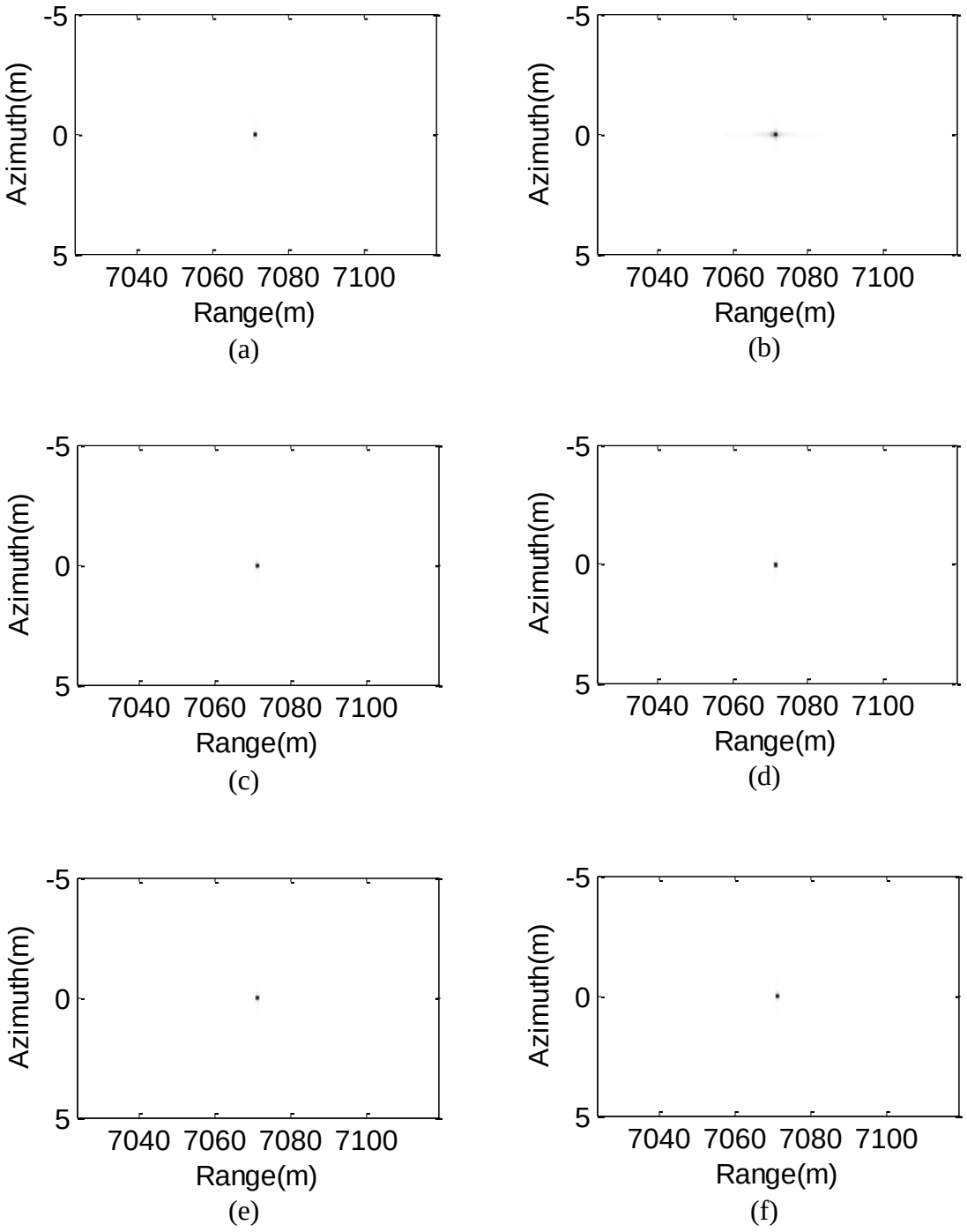

Figure 5.3 Imaging results of synthetic aperture for a single point target. (a) FrFT-based OFDM with 45 degree. (b) FFT-based OFDM. (c) FrFT-based with 35 degree. (d) FrFT-based with 25 degree. (e) FrFT-based OFDM with 15 degree. (f) FrFT-based OFDM with 10 degree.

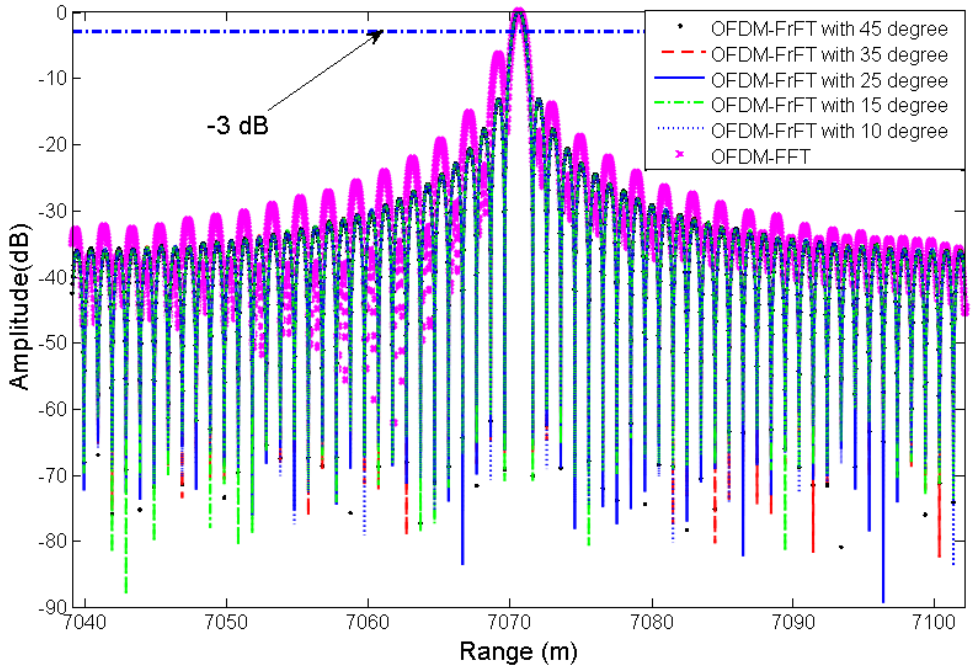

Figure 5.4 Range profiles of the spread function

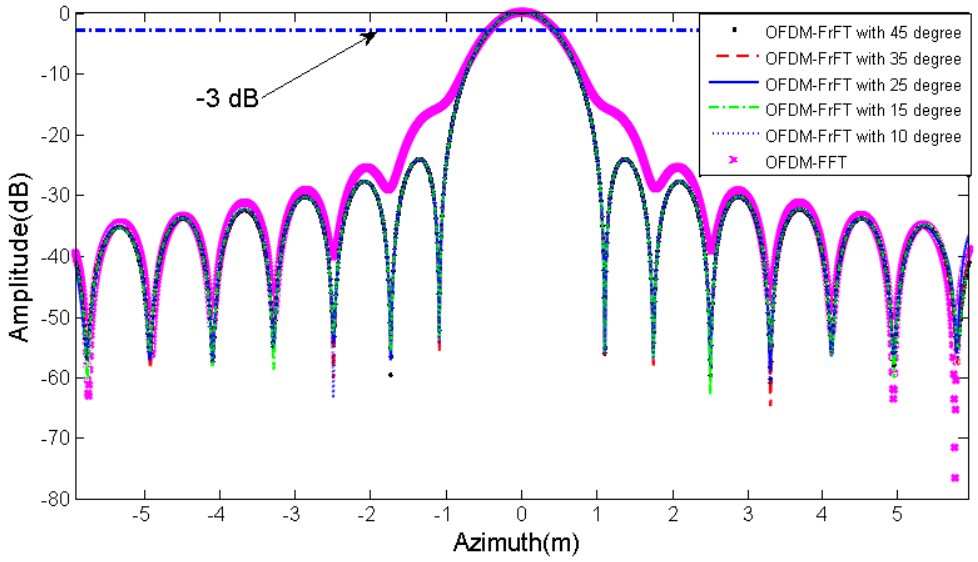

Figure 5.5 Azimuth profiles of the spread function

Table 5-2 Results of quality image metrics

Method	FrFT (45)	FrFT (35)	FrFT (25)	FrFT (15)	FrFT (10)	FFT
$ISLR_{dB}$						
Range	-9.67	-9.69	-9.69	-9.68	-9.68	-5.41
Azimuth	-22.03	-21.98	-22.00	-21.91	-22.04	-22.98
$PSLR_{dB}$						
Range	-13.26	-13.27	-13.24	-13.28	-13.25	-6.51
Azimuth	-24.13	-24.08	-24.14	-24.12	-24.11	-25.51

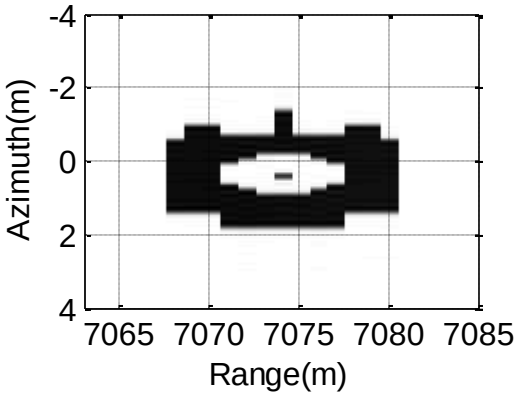

(a)

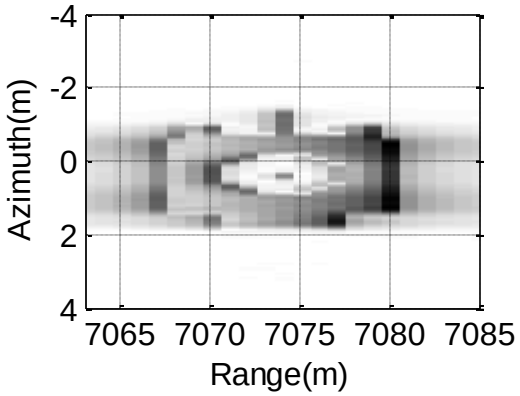

(b)

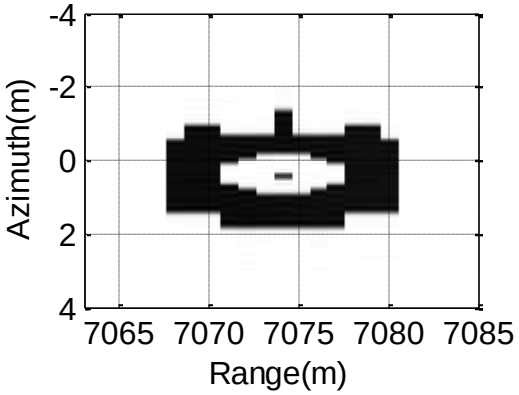

(c)

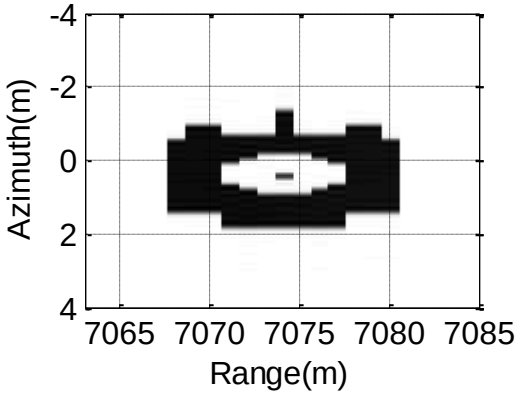

(d)

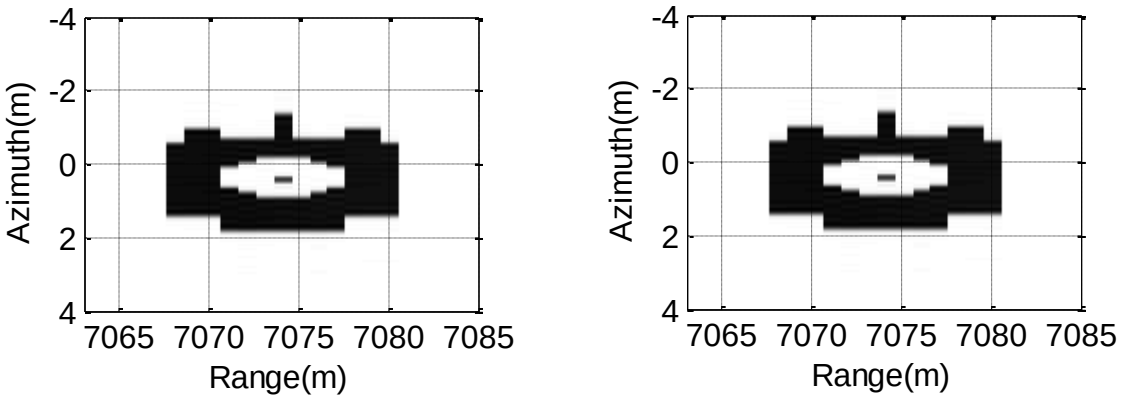

Figure 5.6 Imaging results of synthetic aperture radar for a tank. (a) FrFT-based OFDM with 45 degree tank. (b) FFT-based OFDM tank. (c) FrFT-based OFDM with 35 degree tank. (d) FrFT-based OFDM with 25 degree. (e) FrFT-based OFDM with 15 degree. (f) FrFT-based OFDM with 10 degree

5.5 Chapter Summary

This chapter deals with the developing of monostatic SAR based on the FrFT-based OFDM signal. First of all, the FrFT on which this investigation is basically carried out described briefly with its computation for the application in radar at the transmitter side. Moreover, a method developed for the reconstruction of the range profile that combined with the reconstruction of the cross range profile as used in the range-Doppler algorithm. Furthermore, the performance of this type of signal for SAR has been investigated through the adoption of two types of targets, single point scatterer, and tank. Finally, the range profiles of the point spread function and the azimuth profiles of the point spread function have been obtained from which the quality image metrics has been found such as ISLR and PSLR. It found that the performance of FrFT-based OFDM signal is better than FFT-based OFDM signal for SAR application.

CHAPTER 6

SUMMARY AND CONCLUSION

In this thesis, CP-based OFDM SAR was investigated for FOPEN for the first time where the scene to be observed has two cases, single point target and extended target with the shape of the tank. Furthermore, FrFT-based OFDM signal has been adopted for the first time for SAR application at the transmitter side. Therefore, this chapter concludes what have been accomplished in this thesis and gives a recommendation for a future work.

6.1 Conclusions

This thesis focuses on three aspects regarding the use of OFDM signal for the application in SAR for both single point target and extended target.

Firstly, starting with the elaboration of the adoption of CP–based OFDM signal for SAR by Zhang, the range profile was reconstructed by the estimation of the weighting RCS coefficient at the receiver side instead of the matched filter. However, the number of subcarriers N should be greater than the number of the M cells along the range direction otherwise, it will continue to suffer from the side lobes which are the main contribution into the IRCI. It has been shown that the side lobes of the CP-based OFDM signal are much lower than the side lobes of the other three signals LFM, random noise, and conventional OFDM through the range profiles of the spread function.

Secondly, based on the achieved property of CP-OFDM SAR in obtaining free IRCI, it has been used for the application of FOPEN. The performance of it has been investigated

with the comparison with the random noise signal. The fluctuation of the side lobes for the two signals has been investigated through the range and the azimuth profiles. It has been found that the side lobes of the random noise signal compared to the CP-based OFDM signal for the application of FOPEN fluctuate more. Furthermore, for better clarification, the ISLR, and the PSLR has been investigated for both of the two signals. It was found that the CP-based OFDM signal has lower ISLR and PSLR along the range direction compared to the random noise signal. Therefore, the performance of the CP-based OFDM SAR for the application of FOPEN is better than the random noise SAR.

Thirdly, OFDM signal based on the Fractional Fourier Transform rather than the fast Fourier transform was used for the application of SAR. The received signal at the receiver side has been developed as a linear convolution between the transmitted sequence and the weighting RCS coefficients. After that, the range profile reconstruction was achieved. The processing in the azimuth direction that has been used is similar to the one developed for range Doppler algorithm. We looked into the performance of this signal by varying the angle of the fractional domain using different values, 45 degree, 35 degree, 25 degree, and 10 degree. It was shown that the angle of the fractional domain does not have any effect. Therefore any angle in the fractional domain can be used. Furthermore, we compared the performance of this signal with the FFT-based OFDM signal through the range profiles and the azimuth profiles from which the ISLR and the PSLR have been found. We found that the FrFT-based OFDM signal has lower values of the ISLR and the PSLR along the range direction. As a result, the FrFT-based OFDM signal for SAR has better images than the FFT-based OFDM signal for SAR application.

6.2 Future work

Based on what have been achieved in this thesis, there are possible extensions to what have been accomplished for different applications.

I. Extending the work of CP-based OFDM signal for Bistatic SAR.

II. Taking the advantage of the flexibility in the fractional domain of FrFT-based OFDM signal for SAR in order to reduce the effect of the channel.

III. The use of MIMO FrFT-based OFDM SAR to satisfy the condition of the orthogonality in MIMO SAR through the fractional domain flexibility.

REFERENCES

[1] M. Soumekh, Synthetic Aperture Radar Signal Processing. New York, NY, USA: Wiley, 1999.

[2] Ozdemir, C. Inverse synthetic aperture radar imaging with MATLAB algorithms (Vol. 210). John Wiley & Sons. 2012.

[3] C. W. Sherwin, J. P. Ruina and R. D. Rawcliffe, "Some Early Developments in Synthetic Aperture Radar Systems," in *IRE Transactions on Military Electronics*, vol. MIL-6, no. 2, pp. 111-115, Apr. 1962.

[4] Cumming, I. G., and Wong, F. H. C. Digital processing of synthetic aperture radar data: algorithms and implementation. Artech house. 2005.

[5] Wang, B. C. Digital signal processing techniques and applications in radar image processing (Vol. 91). John Wiley & Sons. 2008.

[6] M. I. Skolnik, Introduction to Radar systems. New York, NY, USA: McGraw-Hill, 2001.

[7] T. Zhang and X. G. Xia, "OFDM Synthetic Aperture Radar Imaging With Sufficient Cyclic Prefix," in *IEEE Transactions on Geoscience and Remote Sensing*, vol. 53, no. 1, pp. 394-404, Jan. 2015.

[8] Curlander, John C., and Robert N. McDonough. Synthetic aperture radar. New York, NY, USA: John Wiley & Sons, 1991.

[9] Richards, Mark A., and William A. Holm. Principles of modern radar. SciTech Pub., 2010.

[10] J. Xuehua and C. Peijiang, "Research and Simulation of MIMO-OFDM Wireless Communication System," *2009 International Forum on Information Technology and Applications*, Chengdu, pp. 83-86, 2009.

[11] Nikookar, Homayoun, and Ramjee Prasad. Introduction to Ultra Wideband for Wireless Communications. Springer Science & Business Media, 2008.

[12] S. R. J. Axelsson, "Analysis of Random Step Frequency Radar and Comparison With Experiments," in *IEEE Transactions on Geoscience and Remote Sensing*, vol. 45, no. 4, pp. 890-904, Apr. 2007.

[13] M. F. Toups, S. Ayasli and J. G. Fleischman, "Analysis of foliage-induced synthetic pattern distortions," in *IEEE Transactions on Aerospace and Electronic Systems*, vol. 32, no. 1, pp. 145-155, Jan. 1996.

[14] Ulaby, F. T., Sarabandi, K., McDonald, K., Whitt, M., and Dobson, M. C. "Michigan microwave canopy scattering model," in International Journal of Remote Sensing, vol. 11, no 7, pp 1223-1253, July 1990.

[15] K. C. Mcdonald, M. C. Dobson and F. T. Ulaby, "Using Mimics To Model L-band Multiangle and Multitemporal Backscatter From A Walnut Orchard," in *IEEE Transactions on Geoscience and Remote Sensing*, vol. 28, no. 4, pp. 477-491, July 1990.

[16] M. A. Karam, F. Amar and A. K. Fung, "Electromagnetic wave scattering from a forest or vegetation canopy: ongoing research at the University of Texas at Arlington," in *IEEE Antennas and Propagation Magazine*, vol. 35, no. 2, pp. 18-26, Apr. 1993.

[17] M. A. Karam, A. K. Fung, R. H. Lang and N. S. Chauhan, "A microwave scattering model for layered vegetation," in *IEEE Transactions on Geoscience and Remote Sensing*, vol. 30, no. 4, pp. 767-784, July 1992.

[18] D. R. Sheen, N. P. Malinas, D. W. Kletzli, T. B. Lewis and J. F. Roman, "Foliage transmission measurements using a ground-based ultrawide band (300-1300 MHz) SAR system," in *IEEE Transactions on Geoscience and Remote Sensing*, vol. 32, no. 1, pp. 118-130, Jan. 1994.

[19] C. Hsu, J. A. Kong, M. F. Toups, J. G. Fleischman, S. Ayasli, and R. T. Shin, "Electromagnetic modeling of foliage obscured point source response, " In Proceedings of SPIE Conference on Underground and Obscured Object Imaging and Detection, vol. 1942, Orlando, FL, pp. 76-87, Nov. 1993.

[20] Xiaojian Xu and R. M. Narayanan, "FOPEN SAR imaging using UWB step-frequency and random noise waveforms," in *IEEE Transactions on Aerospace and Electronic Systems*, vol. 37, no. 4, pp. 1287-1300, Oct. 2001.

[21] N. Levanon, "Multifrequency complementary phase-coded radar signal," in *IEE Proceedings - Radar, Sonar and Navigation*, vol. 147, no. 6, pp. 276-284, Dec. 2000.

[22] G. E. A. Franken, H. Nikookar and P. V. Genderen, "Doppler Tolerance of OFDM-coded Radar Signals," *2006 European Radar Conference*, Manchester, 2006, pp. 108-111.

[23] D. Garmatyuk and J. Schuerger, "Conceptual design of a dual-use radar/communication system based on OFDM," *MILCOM 2008 - 2008 IEEE Military Communications Conference*, San Diego, CA, 2008, pp. 1-7.

[24] D. Garmatyuk, J. Schuerger, K. Kauffman and S. Spalding, "Wideband OFDM system for radar and communications," *2009 IEEE Radar Conference*, Pasadena, CA, 2009, pp. 1-6.

[25] C. Sturm, E. Pancera, T. Zwick and W. Wiesbeck, "A novel approach to OFDM radar processing," *2009 IEEE Radar Conference*, Pasadena, CA, 2009, pp. 1-4.

[26] J. J. M. de Wit, A. Meta and P. Hoogeboom, "Modified range-Doppler processing for FM-CW synthetic aperture radar," in *IEEE Geoscience and Remote Sensing Letters*, vol. 3, no. 1, pp. 83-87, Jan. 2006.

[27] E. C. Zaugg and D. G. Long, "Generalized Frequency-Domain SAR Processing," in *IEEE Transactions on Geoscience and Remote Sensing*, vol. 47, no. 11, pp. 3761-3773, Nov. 2009.

[28] D. Garmatyuk, "Cross-Range SAR Reconstruction With Multicarrier OFDM Signals," in *IEEE Geoscience and Remote Sensing Letters*, vol. 9, no. 5, pp. 808-812, Sept. 2012.

[29] S. Sen and A. Nehorai, "Target Detection in Clutter Using Adaptive OFDM Radar," in *IEEE Signal Processing Letters*, vol. 16, no. 7, pp. 592-595, July 2009.

[30] S. Sen and A. Nehorai, "OFDM MIMO Radar With Mutual-Information Waveform Design for Low-Grazing Angle Tracking," in *IEEE Transactions on Signal Processing*, vol. 58, no. 6, pp. 3152-3162, June 2010.

[31] J. Mittermayer and J. M. Martinez, "Analysis of range ambiguity suppression in SAR by up and down chirp modulation for point and distributed targets," *2003 IEEE International Geoscience and Remote Sensing Symposium*, vol. 6, pp. 4077-4079, 2003.

[32] V. Riché, S. Méric, J. Y. Baudais and É Pottier, "Investigations on OFDM Signal for Range Ambiguity Suppression in SAR Configuration," in *IEEE Transactions on Geoscience and Remote Sensing*, vol. 52, no. 7, pp. 4194-4197, July 2014.

[33] V. Riché, S. Méric, E. Pottier and J. Y. Baudais, "OFDM signal design for range ambiguity suppression in SAR configuration," *2012 IEEE International Geoscience and Remote Sensing Symposium*, Munich, 2012, pp. 2156-2159.

[34] V. Riché, S. Méric, J. Y. Baudais and E. Pottier, "Optimization of OFDM SAR signals for range ambiguity suppression," *Radar Conference (EuRAD), 2012 9th European*, Amsterdam, 2012, pp. 278-281.

[35] T. Zhang, X. G. Xia and L. Kong, "IRCI Free Range Reconstruction for SAR Imaging With Arbitrary Length OFDM Pulse," in *IEEE Transactions on Signal Processing*, vol. 62, no. 18, pp. 4748-4759, Sept.15, 2014.

[36] C. Clemente and J. J. Soraghan, "Range Doppler SAR processing using the Fractional Fourier Transform," *11-th INTERNATIONAL RADAR SYMPOSIUM*, Vilnius, Lithuania, 2010, pp. 1-4.

[37] C. Clemente and J. J. Soraghan, "Fractional RDA and enhanced FrCSA for SAR imaging," *Sensor Signal Processing for Defence (SSPD 2010)*, London, 2010, pp. 1-5.

[38] C. Clemente and J. J. Soraghan, "Range Doppler and chirp scaling processing of synthetic aperture radar data using the fractional Fourier transform," in *IET Signal Processing*, vol. 6, no. 5, pp. 503-510, July 2012.

[39] M.G. El-Mashed, O. Zahran, M.I. Dessouky, M. El-Kordy and F.E. Abd El-Samie, "Synthetic aperture radar imaging with fractional Fourier transform and channel equalization," Digital Signal Processing, Vol. 23, no 1, Jan. 2013.

[40] R. M. Narayanan, X. Xu and J. A. Henning, "Radar penetration imaging using ultra-wideband (UWB) random noise waveforms," in *IEE Proceedings - Radar, Sonar and Navigation*, vol. 151, no. 3, pp. 143-148, 12 June 2004.

VITAE

Ghazal Ali Ba khadher

Saudi Arabia Dammam, KFUPM Dhahran, 31216 Mobile,+966538654645, ghazalphds@gmail.com

Date of Birth: 9th of July 1987 Nationality: Yemeni

Education

- MSc. In Telecommunication Engineering. Electrical Engineering Department. King Fahd University of Petroleum and Minerals (KFUPM), 2016. Saudi Arabia.
- BSc. In Electronics and Communications. Hadhramout University of Science & Technology, 2012. The Republic of Yemen.

Graduate Projects:

- MSc.
  UWB OFDM synthetic aperture radar based on fractional Fourier transform with application to foliage penetration.
- BSc.
  Coverage Planning of CDMA2000.

Publications.

Ghazal A. Ba Khadher and Abdelmalek C. Zidouri. "**OFDM synthetic aperture radar based on fractional Fourier transform**." *2016 13th International Multi-Conference on Systems, Signals & Devices (SSD)*. IEEE, 2016.

Publications under work.

UWB Cyclic Prefix-based OFDM Synthetic Aperture Radar for Foliage Penetration (FOPEN) submitted to *2017 14th International Multi-Conference on Systems, Signals & Devices (SSD). IEEE, 2017.*

Professional Development.

- Introduction to SAP and Navigation (2015).
- Information Technology Essential Course (2012).
- Training at Yemen Mobile Corporation Headquarters located in Sana'a, Yemen (2010).
  CDMA system principle, RF planning principle, BSC and BTS hardware structure

and RF optimization process procedure with practices and practical problems solution.

- Training at Seyion Radio transmission (2009).
  The procedure of transmitting the information from the radio transmitter station.
- Training at Hadhramout Power plant (2009).
  Training the operation room and observation at station II.
  Electrical maintenance of engines and operation of observation the behavior of the engines in the station.
- Participation in the first national university camp at Hadhramout University of Science and Technology, 2008.
  Computer Application Courses – Fist Aid – Guidance skills.

Experience

Simulation.

Synthetic Aperture Radar (SAR) and Inverse Synthetic Aperture Radar (ISAR) Simulation based on Matlab.

Voluntary Work (2012).

Participated in the cleaning of my neighborhood from the waste.

Computer Skills

Microsoft Office Programs

Visio 2016 program

Matlab Program

Latex

Electronics Workbench Program

References

Dr. Abdelmalek Zidouri

IEEE Senior Member, Associate Professor, EE Dept, King Fahd University of Petroleum and Minerals.
malek@kfupm.edu.sa

Dr. Azzedine Zerguine

IEEE Senior Member, Professor, EE Dept, King Fahd University of Petroleum and Minerals. azzedine@kfupm.edu.sa